WILEY InterScience CHIRALITY 19:550–558 (2007)

Stereoselective Hexobarbital 3′-Hydroxylation by CYP2C19 Expressed in Yeast Cells and the Roles of Amino Acid Residues at Positions 300 and 476

KEITA SAITO,[1] HIKARI DAN,[1] KAZUFUMI MASUDA,[2] TAKASHI KATSU,[2] NOBUMITSU HANIOKA,[1] SHIGEO YAMAMOTO,[3] KAZUKO MIYANO,[4] SHIGERU YAMANO,[4] AND SHIZUO NARIMATSU[1]*

[1]*Laboratory of Health Chemistry, Graduate School of Medicine, Dentistry and Pharmaceutical Sciences, Okayama University, Okayama, Japan*

[2]*Laboratory of Pharmaceutical Physical Chemistry, Graduate School of Medicine, Dentistry and Pharmaceutical Sciences, Okayama University, Okayama, Japan*

[3]*Department of Pharmaceutical Health Chemistry, Faculty of Pharmaceutical Sciences, Matsuyama University, Matsuyama, Japan*

[4]*Department of Hygienic Chemistry, Faculty of Pharmaceutical Sciences, Fukuoka University, Fukuoka, Japan*

ABSTRACT We examined the enzymatic function of recombinant CYP2C19 in enantiomeric hexobarbital (HB) 3′-hydroxylation, and searched the roles of amino acid residues, such as Phe-100, Phe-114, Asp-293, Glu-300, and Phe-476 of CYP2C19 in the stereoselective HB 3′-hydroxylation, using a yeast cell expression system and site-directed mutagenesis method. CYP2C19 wild-type exerted substrate enantioselectivity of (*R*)-HB > (*S*)-HB and metabolite diastereoselectivity of 3′(*R*) < 3′(*S*) in 3′-hydroxylation of HB enantiomers. The substitution of Asp-293 by alanine failed to yield an observable peak at 450 nm in its reduced carbon monoxide-difference spectrum. CYP2C19-E300A and CYP2C19-E300V with alanine and valine, respectively, in place of Glu-300 exerted total HB 3′-hydroxylation activities of 45 and 108%, respectively, that of the wild-type. Interestingly, these two mutants showed substrate enantioselectivity of (*R*)-HB < (*S*)-HB, which is opposite to that of the wild-type, while metabolite diasteroselectivity remained unchanged. The replacement of Phe-476 by alanine increased total HB 3′-hydroxylation activity to approximately 3-fold that of the wild-type. Particularly, 3′(*S*)-OH-(*S*)-HB-forming activity elevated to 7-fold that of the wild-type, resulting in the reversal of the substrate enantioselectivity. In contrast, the substitution of phenylalanine at positions 100 and 114 by alanine did not produce a remarkable change in the total activity or the substrate enantioselectivity. These results indicate that Glu-300 and Phe-476 are important in stereoselective oxidation of HB enantiomers by CYP2C19. *Chirality 19:550–558, 2007.* © 2007 Wiley-Liss, Inc.

KEY WORDS: CYP2C19; hexobarbital; enantiomer; substrate enantioselectivity; glutamic acid-300; phenylalanine-476; site-directed mutagenesis

INTRODUCTION

Cytochrome P450 (CYP) is the diverse enzyme superfamily that is responsible for oxidative metabolism of numerous endogenous and exogenous compounds. It is well documented that eight CYP subfamilies, such as CYP1A, CYP2A, CYP2B, CYP2C, CYP2D, CYP2E, CYP3A, and CYP4A, are mainly responsible for the oxidation of chemicals, including medicines.[1,2] Among the drug metabolism-type CYP enzymes, CYP2C19, and CYP2D6 are known as typical enzymes showing extensive genetic polymorphisms.[2–4]

CYP2C19 is a major (*S*)-mephenytoin [(*S*)-MP] 4′-hydroxylase in human livers,[5] and about 20% of Japanese people have deficiencies in normal function.[6] Extensive studies have demonstrated genetic mechanisms causing the lack of CYP2C19 protein or the production of no- or low-functional CYP2C19.[7,8] In addition to (*S*)-MP, more than 30 drugs with various chemical structures have been found to be oxidized by CYP2C19, and hexobarbital (HB) is also one of the substrates of this enzyme.[8] HB has an asymmetric carbon atom at 5-position of the barbituric acid structure, yielding (*S*)- and (*R*)-enantiomers (Fig. 1).

© 2007 Wiley-Liss, Inc.

Abbreviations: BF, bufuralol; CYP, cytochrome P450; fp_2, NADPH-cytochrome P450 reductase; G-6-P, glucose 6-phosphate; HB, hexobarbital; HPLC, high-performance liquid chromatography; 1″-OH-BF, 1″-hydroxybufuralol; 3′-OH-HB, 3′-hydroxyhexobarbital; (*S*)-MP, (*S*)-mephenytoin.

Contract grant sponsor: Ministry of Education, Sports, Science, and Technology of Japan; Contract grant numbers: 17390035.

*Correspondence to: Prof. Shizuo Narimatsu, Laboratory of Health Chemistry, Graduate School of Medicine, Dentistry and Pharmaceutical Sciences, Okayama University, 1-1-1 Tsushima-naka, Okayama 700-8530, Japan.

Received for publication 18 December 2006; Accepted 5 March 2007
DOI: 10.1002/chir.20412
Published online 8 May 2007 in Wiley InterScience (www.interscience.wiley.com).

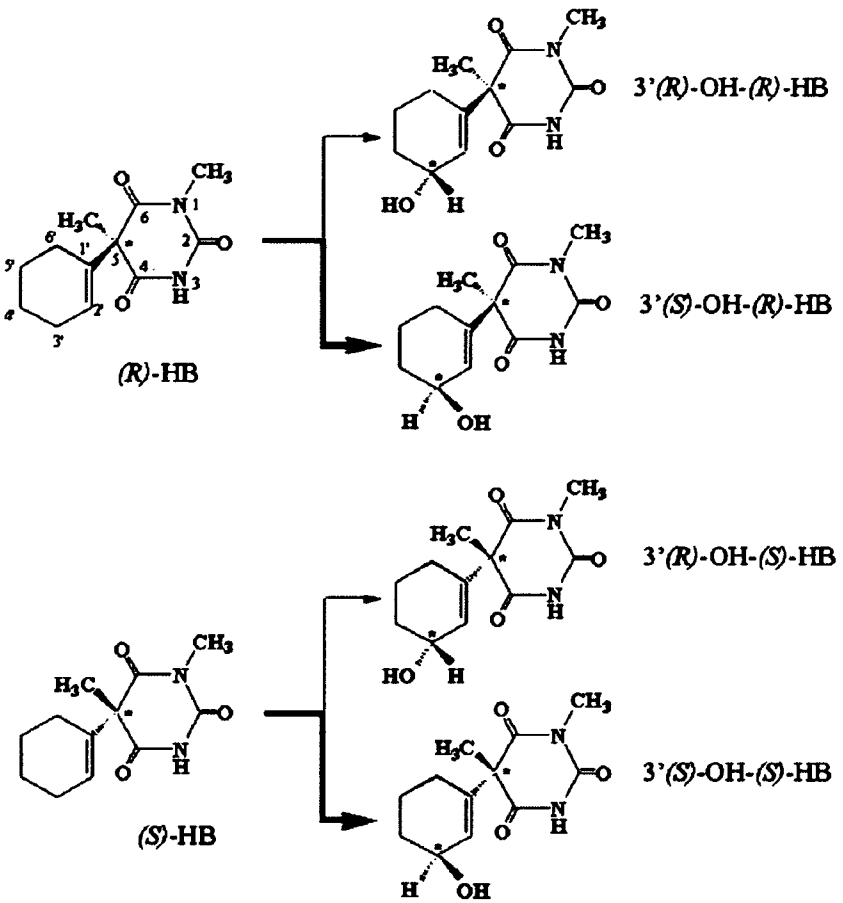

Fig. 1. 3'-Hydroxylation of the cyclohexenyl ring of HB enantiomers. *Asymetric carbon atom.

For in vivo information on stereoselective HB metabolism in humans, Adedoyin et al.[9] observed that oral clearance of (*R*)-HB is several times higher than that of (*S*)-HB in extensive metabolizers of (*S*)-MP. For in vitro information, Yasumori et al.[10] described that human liver microsomes from extensive metabolizers of (*S*)-MP favored (*S*)-HB over (*R*)-HB as a substrate, and recombinant CYP human-2 yielded the same substrate enantioselectivity. However, the recombinant human-2 used in their investigation was CYP2C9[11] but not CYP2C19, the major (*S*)-MP 4'-hydroxylase. Therefore, there has been no reliable in vitro information to date on the stereoselective oxidation of HB enantiomers by CYP2C19.

In our previous studies,[12–14] we established high-performance liquid chromatographic methodology to efficiently separate four diastereomers of 1″-hydroxybufuralol (1″-OH-BF) formed from bufuralol (BF) racemate. In that study, we examined BF 1″-hydroxylase activities of four human liver microsomal fractions, all of which showed substrate enantioselectivity of (*R*)-BF > (*S*)-BF. Interestingly, 3 of the 4 human liver microsomal fractions exhibited metabolite diastereoselectivity of 1″(*R*)-OH-BF < 1″(*S*)-OH-BF, whereas only one fraction showed reversed selectivity of 1″(*R*)-OH-BF > 1″(*S*)-OH-BF. Using recombinant CYP enzymes, we demonstrated that CYP2D6 and CYP2C19 yielded the metabolite diastereoselectivity of 1″(*R*)-OH-BF < 1″(*S*)-OH-BF and 1″(*R*)-OH-BF > 1″(*S*)-OH-BF, respectively, whereas they exerted the same substrate enantioselectivity of (*R*)-BF > (*S*)-BF.[12,13]

A question arises about what causes the reversed selectivity between CYP2D6 and CYP2C19 for 1″-hydroxylation of BF enantiomers. In other words, what amino acid residues in the active sites of the two enzymes are involved in and how do they contribute the reversed selectivity? We obtained the conformation of CYP2C19 protein that was constructed in silico, using the crystal structures of CYP2C9.[15] Recently, Rowland et al.[16] succeeded in crystallization of CYP2D6. In the active-site cavity of CYP2D6, Phe-120, Glu-216, Asp-301, and Phe-483 are thought to have important roles in the oxidation of the substrates.[16–18] Moreover, Melet et al.[19] described the importance of Phe-114, Ser-365, and Phe-476 in the active-site cavity of CYP2C9, which shows high identity of 91% with CYP2C19 in their amino acid sequences. Through careful compari-

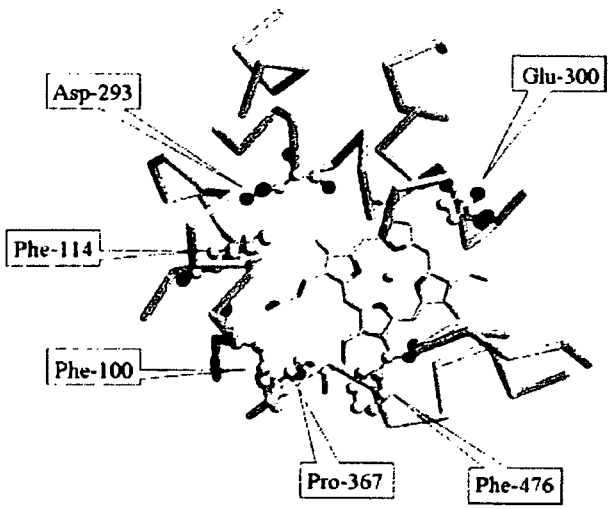

Fig. 2. The conformation of the active-site cavity of CYP2C19. Amino acid residues to be discussed are depicted as the "ball and stick" form with RasMol version 2.6-ucb-1.0. [Color figure can be viewed in the online issue, which is available at www.interscience.wiley.com]

son of the structures of CYP2C19, CYP2D6, and CYP2C9, we chose Phe-100, Phe-114, Asp-293, Glu-300, and Phe-476 of CYP2C19 to be replaced with another amino acid residue (Fig. 2).

It is well known that most of the substrates for CYP2D6 have a basic nitrogen atom in their chemical structure. It has been proposed that the carboxylate group of Glu-216 located in the F-helix in the active-site of CYP2D6 makes an ionic interaction with the basic nitrogen atom of the substrate and oxidation site is 5–7 Å apart from the nitrogen atom.[20] In the active-site of CYP2C19, however, there is no acidic amino acid in the F-helix, corresponding to Glu-216 of CYP2D6. Instead, Glu300 is located in the I-helix. This acidic amino acid may have some role(s) in the stereoselective oxidation of chiral substrates, including BF by CYP2C19.

We thus conducted the present study 1) to examine enzymatic function of recombinant CYP2C19 in the oxidation of HB enantiomers, and 2) to evaluate the roles of the amino acid residues in the active-site cavity of CYP2C19 in the stereoselective oxidation of HB. For this, we prepared cDNAs encoding six CYP2C19 mutants (CYP2C19-F100A, -F114A, -D293A, -E300D, -E300V, and -F476A), and expressed their proteins in a yeast cell expression system. The functions of the mutants for the oxidation of HB enantiomers were compared with those of CYP2C19 wild-type in the present study.

MATERIALS AND METHODS

Materials

Sodium HB enantiomers and 3′(*R*)- and 3′(*S*)-hydroxyhexobarbital (3′-OH-HB) racemates were supplied from Dr. Toki, Fukuoka University (Fukuoka, Japan). Because HB enantiomers showed over 99% purities in HPLC analysis, we used them as substrates without further purification. Glucose 6-phosphate (G-6-P) dehydrogenase (from yeast) and NADPH were from Wako Pure Chemical (Osaka, Japan); Emulgen 911 was from Kao (Tokyo, Japan). Other chemical reagents or solvents used were of the highest quality commercially available.

Construction of CYP Expression Plasmids

CYP2C19 cDNA cloned into pBluescript-SK(±) vector (pBluescript/CYP2C19) was kindly provided by Dr. Joyce A. Goldstein, National Institute of Environmental Health Sciences (Research Triangle Park, NC). CYP2C19 cDNA was amplified by polymerase chain reaction from pBluescript/CYP2C19 as a template, using the forward primer 5′-CCCAAGCTTAAAAAAATGGATCCTTTTGTGGTCC-3′ and the reverse primer 5′-GGAAAGCTTAGGAGCAGC-CAGACCATCTGT-3′. *Hin*dIII sites (marked with the solid line) were introduced to the 5′-end of the start codon and the 3′-end of the stop codon to facilitate subcloning into pGYR1, which has a glyceraldehyde-3-dehydrogenase promoter and the yeast NADPH-CYP reductase (fp_2) gene. A yeast consensus sequence[21] (marked with dotted line) was also introduced upstream of the start codon to achieve a high expression of protein in yeast cells. The PCR product thus obtained was digested with *Hin*dIII and ligated into the same restriction enzyme site of pcDNA3.1(+), resulting in pcDNA3.1/CYP2C19. The pcDNA3.1/CYP2C19 plasmid was sequenced in both forward and reverse directions, using a BigDye terminator cycle sequencing reaction kit v3.1 (Applied Biosystems, Foster City, CA) to confirm that there were no PCR errors. The mutated CYP2C19 cDNAs (F100A, F114A, D293A, E300D, E300Q, E300V, and F476A) were constructed with QuikChange site-directed mutagenesis kit (Stratagene, La Jolla, CA), using pcDNA3.1/CYP2C19 as a template. The sets of forward and reverse primers are listed in Table 1. To ensure that no errors had been introduced during the amplification process, the plasmids were verified by DNA sequencing of both strands. The cDNA fragments corresponding to CYP2C19 wild-type and mutants were cut out with *Hin*dIII from the pcDNA3.1 plasmids, and were subsequently subcloned into the pGYR1 yeast expression vector digested with *Hin*dIII. The expression plasmids were sequenced to verify the correct orientation with respect to the promoter for pGYR1.

Expression of CYPC19 and its Mutants in Yeast Cells

Yeast cells, *Saccharomyces cerevisiae* AH22, were transformed with the pGYR1 vectors containing each of cDNAs encoding CYP2C19 wild-type and its mutants by the lithium method, and yeast transformants thus obtained were cultivated according to the published procedure.[22] Microsomes from yeast cells were prepared as described previously.[23] Appropriate portions of the microsomal fractions thus obtained were diluted with 100 mM potassium phosphate buffer (pH 7.4) containing 20% glycerol and 0.2% Emulgen 911 (10 mg protein/ml). Total contents of holo-CYP proteins were spectrophotometrically measured based on reduced carbon monoxide (CO)-difference spec-

TABLE 1. Primers used for site-directed mutagensis

Primer	Sequence
F100A-F	5′-GGAAGAGGCCAT**GCC**CCACTGGCTGAAAGAG-3′
F100A-R	5′-CTCTTTCAGCCAG**TGG**G**GC**ATGGCCTCTTCC-3′
F114A-F	5′-GAGGATTTGGAATCGT**TGC**CAGCAATGGAAAGAGATGGAAGGAG-3′
F114A-R	5′-CTCCTTCCATCTCTTTCC**ATT**GCT**GG**CAACGATTCCAAATCCTC-3′
D293A-F	5′-GGTAATCACTGCAGCT**GCC**TTACTTGGAGCTGGG-3′
D293A-R	5′-CCCAGCTCCAAGTAA**GGC**AGCTGCAGTGATTACC-3′
E300A-F	5′-CTTACTTGGAGCTGG**GAC**AG**CC**ACAACAAGCACAACCCTGAG-3′
E300A-R	5′-CTCAGGGTTGTGCTTGTTGT**GGC**TGTCCCAGCTCCAAGTAAG-3′
E300V-F	5′-CTTACTTGGAGCTGGGACAG**TA**ACAACAAGCACAACCCTGAG-3′
E300V-R	5′-CTCAGGGTTGTGCTTGTTGT**TAC**TGTCCCAGCTCCAAGTAAG-3′
F476A-F	5′-CAACTCCTGTTGTCAATGGA**GCC**GCTTCTGTCCCGCCCTTC-3′
F476A-R	5′-GAAGGGCGGGACAGAAGC**GGC**TCCATTGACAACAGGAGTTG-3′

Bold and underlined letters indicate the mutation sites introduced by PCR-based mutagenesis.

trum by the method of Omura and Sato, using 91 mM^{-1} cm^{-1} as an absorption coefficient.[24]

Enzyme Assay

HB 3′-hydroxylase activity in microsomal fractions from yeast cells expressing CYP2C19 or its mutants was determined according to the published method[10] with a slight modification. Briefly, the ice-cold incubation mixture (500 μl) in a conical glass tube (10 ml) with a stopper contained 5 mM G-6-P, 1 IU of G-6-P dehydrogenase, 5 mM $MgCl_2$, 0.1 mM EDTA, 0.5 mM NADPH, and HB enantiomer (5–1000 μM). After preincubation at 37°C for 5 min, the reaction was started by adding the microsomal fraction (20 pmol CYP) and was stopped 5 min later by adding 3 ml of dichloromethane and vortexing. Then 4 nmol of phenobarbital was added as an internal standard, and the mixture was shaken vigorously, and centrifuged at 1,200*g* for 15 min. The organic layer (2 ml) was taken, and evaporated in vacuo, and the residue was dissolved in 200 μl of methanol/water (1:1, by volume). An aliquot (10 μl) was subjected to HPLC under the conditions described later. Calibration curves of four kinds of 3′-OH-HB metabolites were made by spiking known amounts of the synthetic compounds in an ice-cold reaction medium, followed by adding dichloromethane (3 ml) and treated as described earlier. The detection limits for 3′(*R*)-OH-(*R*)-HB and 3′(*S*)-OH-(*S*)-HB were 10 pmol/ml, and those for 3′(*S*)-OH-(*R*)-HB and 3′(*R*)-OH-(*S*)-HB were 20 pmol/ml with a signal-to-noise ratio of 3. The intra- and inter-day variation coefficients did not exceed 10% in any assay. Kinetic parameters (apparent K_m and V_{max} values) were estimated by analyzing Michaelis–Menten plots, using the computer program Prism ver. 4.0 software (GraphPad Software, San Diego, CA).

HPLC Conditions

The HPLC conditions were as follows: a Tosoh liquid chromatograph equipped with a DP-8020 pump, an AS-8021 autosampler, a CO-8020 column oven, a UV-8020 variable wavelength UV monitor, a GT-102 degasser, and a Shimadzu C-R3A Chromatopac data processor; column, Inertsil ODS-80A (4.6 × 150 mm, GL Science, Tokyo, Japan) at 40°C. The mobile phase used for HB 3′-hydroxylation was a linear gradient system consisting of (A) 3.5 mM NaH_2PO_4 (pH 2.7)/acetonitrile/methanol (82:5:13, by volume) and (B) 3.5 mM NaH_2PO_4(pH 2.7)/acetonitrile/methanol (57:25:18, by volume) as follows; 0–10 min, (A) 100%; 10–14 min, from (A) 100% to (A)/(B) = 60/40; 14–26 min, from (A)/(B) = 60/40 to (B) 100%; 26–30 min, (B) 100%; 30–31 min, from (B) 100% to (A) 100%; 31–40 min, (A) 100% at a flow rate of 1.0 ml/min (detection, 220 nm). Retention times under the present conditions were: 3′(*S*)-OH-(*R*)-HB 6.9 min, 3′(*R*)-OH-(*R*)-HB 7.8 min, (*R*)-HB 22.7 min, 3′(*S*)-OH-(*S*)-HB 7.0 min, 3′(*R*)-OH-(*S*)-HB 7.8 min, (*S*)-HB 22.8 min, phenobarbital (i.s.) 16.7 min.

Molecular Modeling

The conformation of CYP2C19 was automatically constructed by Swiss-Model (http://swissmodel.expasy.org/), using the crystallographic data of CYP2C9 (1OG5) obtained from Protein Data Bank (http://www.rcsb.org/pdb/). Six peptides of CYP2C19 (Arg-97 to Asn-116, Met-198 to Ser-209, Leu-234 to Phe-239, Ile-289 to Ser-303, Ile-359 to His-368, and Thr-469 to Ser-478) were extracted as substrate recognition sites. Energy optimization of the model was performed using Insight II/Discover as described previously.[14] The amino acid residues at the active sites of CYP2C19 were drawn using RasMol version 2.6-ucb-1.0 as reported previously.[14]

RESULTS

Functional P450 Contents

Yeast cell microsomal fraction expressing CYP2C19 wild-type gave a typical reduced CO-difference spectrum having a Soret peak at 450 nm and practically no peak at 420 nm (spectra of the wild-type and mutants are not shown). Although CYP2C19 mutants with alanine (CYP2C19-E300A) and valine (CYP2C19-E300V) in place of Glu-300 also yielded typical reduced CO-difference spectra, the CYP contents were one-half that of the wild-type. In contrast, CYP2C19 mutant with alanine in place of Asp-293 (CYP2C19-D293A) yielded no observable peaks at 450 or 420 nm in the CO-difference spectrum. The content of

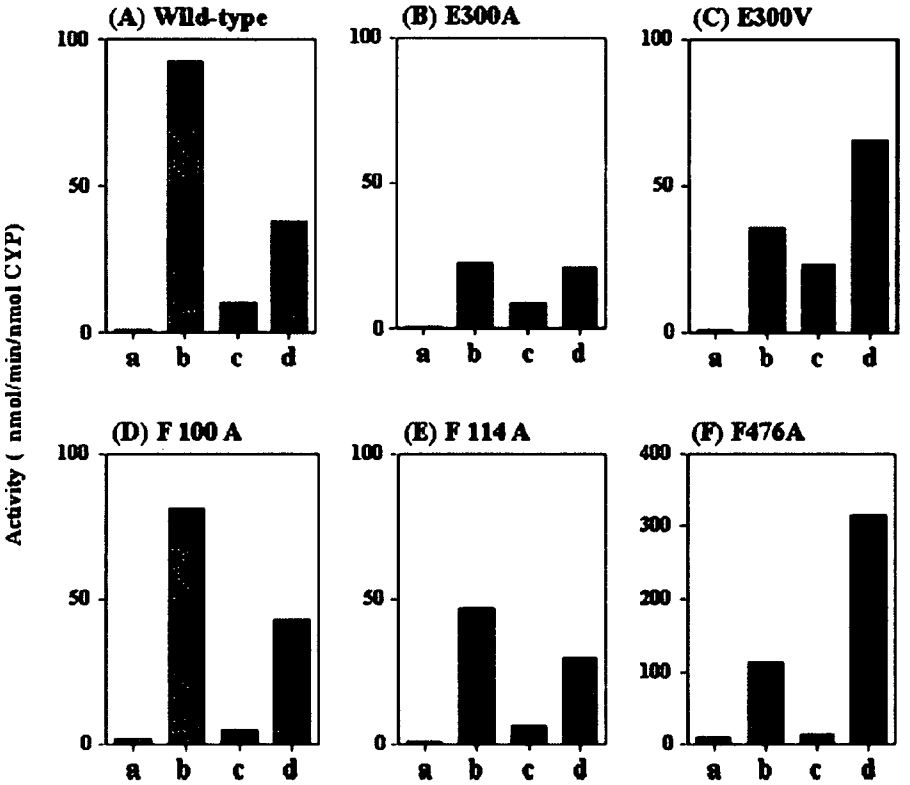

Fig. 3. Comparison of stereoselective HB 3′-hydroxylase activities among CYP2C19 wild-type and its five mutants. The substrate concentration used was 500 μM. Each value represents the mean of two independent determinations. a, 3′(*R*)-OH-(*R*)-HB; b, 3′(*S*)-OH-(*R*)-HB; c, 3′(*R*)-OH-(*S*)-HB; d, 3′(*S*)-OH-(*S*)-HB.

each recombinant CYP2C19 enzyme was as follows: CYP2C19 wild-type, 41.4 pmol/mg protein; CYP2C19-E300A, 16.7 pmol/mg protein; CYP2C19-E300V, 31.9 pmol/mg protein; CYP2C19-F100A, 20.0 pmol/mg protein; CYP2C19-F114A, 28.0 pmol/mg protein; CYP2C19-F476A, 17.6 pmol/mg protein (each value represents the mean of two independent preparations). In a previous study,[25] we confirmed that almost constant level of fp_2 (60–100 pmol/mg microsomal protein) expressed in the yeast cell expression system employed, meaning that the mol ratio of fp_2 to CYP is about 1.5 to 1 in the present study.

Enantiomeric HB 3′-Hydroxylation by CYP2C19 and its Mutants

When the substrate concentration of 500 μM was employed, CYP2C19 wild-type and its five mutants except for CYP2C19-D293A showed enantiomeric HB 3′-hydroxylase activities (Fig. 3). CYP2C19-D293A did not produce any metabolites in detectable amounts under the conditions employed. As shown in Figure 3A, CYP2C19 wild-type exerted substrate enantioselectivity of (*R*)-HB (a + b) > (*S*)-HB (c + d), where a, b, c, and d are 3′(*R*)-OH-(*R*)-HB, 3′(*S*)-OH-(*R*)-HB, 3′(*R*)-OH-(*S*)-HB, and 3′(*S*)-OH-(*S*)-HB, respectively.

Furthermore, Figure 3A also shows product enantioselectivity of 3′*R* < 3′*S* in enantiomeric HB 3′-hydroxylation at the same time. CYP2C19-E300A (Fig. 3B) and CYP2C19-E300V (Fig. 3C) with alanine and valine, respectively, in place of Glu-300 exerted total HB 3′-hydroxylation activities of 45 and 108%, respectively, as that of the wild-type. Interestingly, these two mutants showed substrate enantioselectivity of (*R*)-HB < (*S*)-HB, which is opposite to that of the wild-type, while metabolite diaseteroselectivity remained unchanged.

A much more pronounced effect was observed for CYP2C19-F476A (Fig. 3F). The replacement of Phe-476 by alanine increased total HB 3′-hydroxylation activities to approximately 3-fold that of the wild-type, particularly 3′(*S*)-OH-(*S*)-HB-forming activity was substantially elevated to 7-fold that of the wild-type, resulting in the reversal of the substrate enatioselectivity from [(*R*)-HB:(*S*)-HB = 1:0.5] for the wild-type to [(*R*)-HB:(*S*)-HB = 0.4:1] for the mutant (Fig. 3F). In contrast, the replacement of Phe-100 and Phe-114 with alanine affected neither substrate enantioselectivity nor metabolite diastereoselectivity (Figs. 3D and 3E), whereas the total activities tended to be decreased.

Kinetics

Table 2 summarizes calculated kinetic parameters. As for apparent K_m values, the substitution of Glu-300 by alanine and valine did not change this parameter. The

TABLE 2. Kinetic parameters for enantiomeric HB 3′-hydroxylation by CYP2C19 wild-type and its mutants

CYP2C19	K_m(μM)	V_{max} (nmol/min/nmol CYP)	V_{max}/K_m (μl/min/nmol CYP)
Wild-type			
a	45 ± 27	0.8 ± 0.4	19.3 ± 3.2
b	65 ± 7	92.7 ± 32.8	1420 ± 430
c	187 ± 14	10.1 ± 3.4	54 ± 15
d	183 ± 14	38.0 ± 10.6	207 ± 51
E300A			
a	45 (1.0)	0.6 (0.6)	13.8 (0.2)
b	49 (0.7)	19.8 (0.2)	404 (0.3)
c	276 (1.5)	12.8 (1.3)	46.4 (0.8)
d	255 (1.4)	30.1 (0.8)	118 (0.6)
E300V			
a	37 (0.8)	0.8 (1.0)	22.6 (1.2)
b	54 (0.8)	35.9 (0.4)	663 (0.5)
c	194 (1.0)	23.2 (2.3)	120 (2.2)
d	182 (1.0)	65.5 (1.7)	359 (1.7)
F100A			
a	364 (8.1)	1.7 (2.1)	5.1 (0.3)
b	217 (3.3)	80.7 (0.9)	383 (0.3)
c	1230 (6.6)	5.0 (0.5)	4.7 (0.1)
d	840 (4.6)	43.0 (1.1)	55.7 (0.3)
F114A			
a	153 (3.4)	1.0 (1.3)	6.6 (0.3)
b	104 (1.6)	46.9 (0.5)	451 (0.3)
c	193 (1.0)	6.5 (0.6)	33.5 (0.6)
d	190 (1.1)	29.9 (0.8)	157 (0.8)
F476A			
a	807 (17.9)	8.5 (10.6)	10.9 (0.6)
b	457 (7.0)	114 (1.2)	259 (0.2)
c	306 (1.6)	13.6 (1.3)	44.8 (0.8)
d	248 (1.4)	313 (8.2)	1256 (6.0)

a, 3′ (*R*)-OH(*R*)-HB; b, 3′(*S*)-OH-(*R*)-HB; c, 3′ (*R*)-OH-(*S*)-HB; d, 3′(*S*)-OH-(*S*)-HB.
The values of the wild-type are the mean ± SD ($n = 3$). Each value except for the wild-type represents the mean of two independent determinations. Values in parentheses show the ratio to the value of the wild-type taken as 1.0.

replacement of Phe-476 and Phe-100 with alanine substantially increased K_m values, particularly for (*R*)-HB 3′-hydroxylation. By the substitution of amino acid residue at positions 300 and 476, in general, K_m values for (*R*)-HB oxidation tended to be increased, while K_m values for (*S*)-HB 3′-hydroxylation tended to be relatively constant. As for V_{max} values, the parameters reflected the profile of Figure 3, showing the activities at a substrate concentration of 500 μM.

DISCUSSION

In the first stage of the present study, we examined enantiomeric HB 3′-hydroxylation by recombinant CYP2C19 expressed in yeast cells. HB is a chiral compound, and 3′-hydroxylation of the cyclohexenyl ring yields a new chiral center, resulting in the formation of four diastereomers from HB enantiomers; 3′(*R*)-OH-(*R*)-HB, 3′(*S*)-OH-(*R*)-HB, 3′(*R*)-OH-(*S*)-HB, and 3′(*S*)-OH-(*S*)-HB (Fig. 1). The research group of Toki, Fukuoka University, has been studying the metabolic fate of HB enantiomers (mainly HB oxidation and 3′-OH-HB dehydrogenation) in various experimental animal species for a long time (refer to the reviews of Takenoshita and Toki[26] and the references cited therein). Miyano et al.[27] demonstrated that rat liver microsomes showed substrate enantioselectivity of (*R*)-HB < (*S*)-HB and metabolite diastereoselectivity of 3′*R* < 3′*S* in 3′-hydroxylation of HB enantiomers. Prior to the current study, we also confirmed these selectivities in a preliminary experiment, using rat liver microsomes and the HB metabolites supplied by Dr. Toki.

Although many studies have been reported to date on the metabolic profiles of HB enantiomers (refer to Literature Cited 9, 10, 26 and the references cited therein), to our best knowledge, this is the first report on the stereoselective 3′-hydroxylation of HB enantiomers by recombinant CYP2C19, using authentic 3′-OH-HB samples. Interestingly, CYP2C19 in the present yeast cell expression system showed a substrate enantioselectivity of (*R*)-HB > (*S*)-HB, which is opposite to the reported selectivity [(*R*)-HB < (*S*)-HB] of rat[26] and human liver microsomal fractions.[10] Moreover, the recombinant CYP2C19 exerted the same metabolite diastereoselectivity (3′*R* < 3′*S*) for enantiomeric HB 3′-hydroxylation as that of the rat[27] and human liver microsomes.[10]

Yasumori et al. cloned the cDNA encoding P450 human-2 (CYP2C9)[11] but not CYP2C19. At that time, they believed that the P450 human-2 was the major CYP enzyme responsible for HB 3′-hydroxylation as well as for (*S*)-MP 4′-hydroxylation. If the human livers, which they employed, contained CYP2C9 as the major CYP2C enzymes, it is reasonable that the human liver microsomal fractions they used showed the same enantioselectivity as that of the P450 human-2 (CYP2C9) in enantiomeric HB 3′-hydroxylation. However, not a few researchers who read the papers of Yasumori et al.[10,11] have mistakenly understood that the major (*S*)-MP 4′-hydroxylase, namely CYP2C19, showed the enantioselectivity of (*R*)-HB < (*S*)-HB.[8] The present results will clear up the misunderstanding.

As described in the Introduction section, CYP2C19 catalyzes BF 1″-hydroxylation like CYP2D6, but its metabolite diastereoselectivity is opposite to that of CYP2D6, although the total activity of CYP2C19 was much lower than that of CYP2D6.[12] In the oxidation reaction by CYP2D6, the substrates with basic nitrogen atom(s) are thought to be ionically captured by the carboxylate groups of acidic amino acids located in the active-site cavity.[13] We hypothesized that CYP2C19 also catalyzes BF 1″-hydroxylation in a similar manner. In the second stage of the current study, we thus chose Asp-293 and Glu-300 as key acidic amino acid residues to be replaced with another amino acid in the active-site cavity of CYP2C19 to determine their roles in the stereoselective oxidation of HB enantiomers. As an amino acid to replace the residues at positions 293 and 300, we employed alanine having a methyl group with the smallest size among the various side-chains of amino acids.

The substitution of Asp-293 by alanine failed to yield observable Soret peaks at 450 and 420 nm in the reduced CO-difference spectrum. A similar phenomenon was

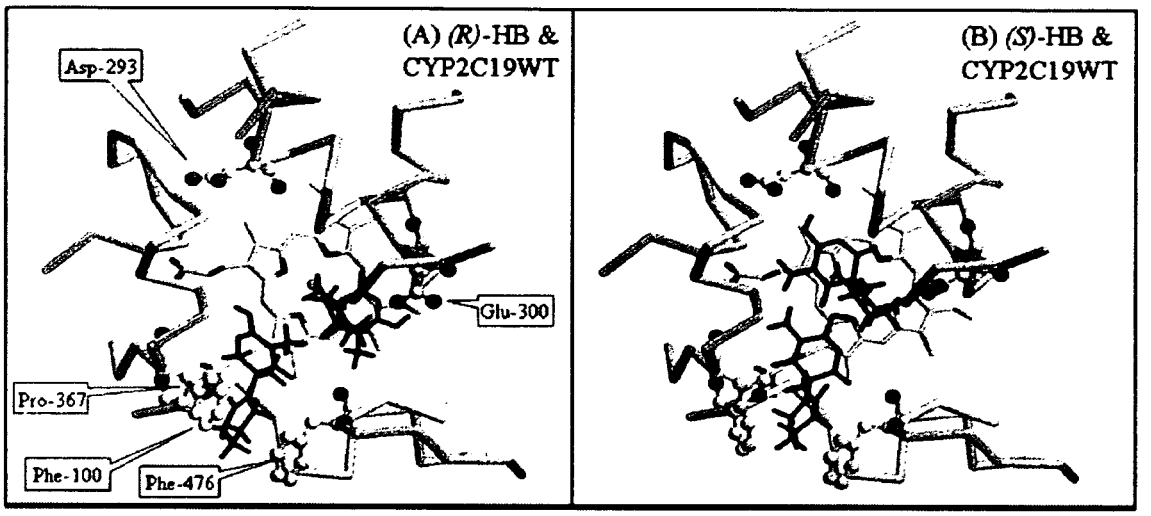

Fig. 4. Possible modes of interaction between HB enantiomers and amino acid residues in the active-site cavity of CYP2C19. Phe-100, Asp-293, Glu-300, Pro-367, and Phe-476 are depicted as "ball and stick" form, and HB is as "stick" form with RasMol version 2.6-ucb-1.0. [Color figure can be viewed in the online issue, which is available at www.interscience.wiley.com]

observed for CYP2D6; i.e., the substitution of Asp-301 by alanine substantially decreased the Soret peak at 450 nm in the reduced CO-difference spectrum of the CYP2D6 mutant.[17,18] In the active-site cavity of CYP2D6, Asp-301 is thought to have a role of appropriately holding the active-site conformation via hydrogen-bonding with the backbone NH of B′-C loop.[16,18] Therefore, it is likely that Asp-293 of CYP2C19 has a role similar to that of Asp-301 of CYP2D6.

The substitution of Glu-300 by alanine caused a marked decreased (*R*)-HB 3′-hydroxylation activities, particularly the activity of 3′(*S*)-OH-(*R*)-HB formation, which caused the reversal of the substrate enantioselectivity from (*R*)-HB > (*S*)-HB to (*R*)-HB < (*S*)-HB without alteration of diastereoselectivity in the formation of metabolites. The replacement of Glu-300 with valine having a more bulky side-chain as compared with alanine decreased (*R*)-HB 3′-hydroxylation activities concomitantly with the elevation of (*S*)-HB 3′-hydroxylation activities, resulting in a more pronounced reversal of the substrate enantioselectivity.

Williams et al.[15] obtained crystal structures of CYP2C9 both unliganded and in complex with (*S*)-warfarin, a typical substrate of CYP2C9. They proposed the existence of a new pocket to which an (*S*)-warfarin molecule is accommodated and there is space for another (*S*)-warfarin molecule to interact with the heme iron. The phenyl group of (*S*)-warfarin was shown to be packed against the hydrophobic binding-site that was composed of Phe-100, Pro-367, and Phe-476.[15] The active-site conformations are thought to be very similar between CYP2C9 and CYP2C19, indicating the existence of a similar binding site also in the active-site cavity of CYP2C19.

As shown in Figure 2, CYP2C19 has phenylalanine residues at positions of 100, 114, and 476 whose locations are relatively close each other in the active-site cavity. In the third stage of the present study, we examined the roles of Phe-100, Phe-114, and Phe-476, probably composing the hydrophobic binding-site, in the oxidation of HB enantiomers by CYP2C19. We thus substituted each of the residues by alanine having an alkyl side-chain with a much smaller size as compared with the phenyl ring, because a marked change in the size of the side-chain may affect the substrate enantioselectivity or metabolite diastereoselectivity in the HB oxidation by CYP2C19.

Although the replacement of the residues at 100 and 114 did not produce a remarkable change in enantiomeric HB 3′-hydroxylation activities, the substitution of Phe-476 with alanine substantially increased 3′(*S*)-OH-(*S*)-HB-forming activity approximately 10-fold that of the wild-type, whereas other three activities did not change so much, which caused the reversal of substrate enantioselectivity from (*R*)-HB > (*S*)-HB for CYP2C19 wild-type to (*R*)-HB < (*S*)-HB for CYP2C19-F476A (Fig. 3G). The extent of the reversal is much higher in CYP2C19-F476A than in CYP2C19-E300A and CYP2C19-E300V. These results indicate that HB enantiomers interact with Phe-476.

Then, what mechanism causes the reversal of substrate enantioselectivity in HB 3′-hydroxylation by CYP2C19 and its mutants in the current study? Our speculation is as follow. If HB interacts with Glu-300 in the active-site cavity of CYP2C19, it is feasible that the carbonyl group at position 2 or the nitrogen atom at position 3 of HB forms a hydrogen-bond with the carboxylate group of Glu-300 or Asp-293, resulting in the orientation where the oxidation site (3′-position) of the cyclohexenyl ring of HB spacially comes close to the heme iron. (*R*)-HB is captured preferentially by Glu-300 rather than by Asp-293, yielding the selectivity of 3′(*R*)-OH-(*R*)-HB < 3′(*S*)-OH-(*R*)-HB, whereas (*S*)-HB is preferentially trapped by Asp-293 rather than by Glu-300, giving the selectivity of 3′(*R*)-OH-(*S*)-HB < 3′(*S*)-OH-(*S*)-HB.

The substrate is thought to enter into the active-site cavity from the upper-right direction in Figure 2. In this situa-

tion, the substrate has a chance to first encounter the carboxylate group of Glu-300 (see Fig. 4). In the case of (*R*)-HB, the interaction with Glu-300 may give a much higher 3′(*S*)-hydroxylation activity as compared with the interaction with Asp-293, favoring 3′(*R*)-hydroxylation. The substrate, which escapes from interaction with Glu-300, may be packed against the hydrophobic binding-site. If the substrate is not trapped by the hydrophobic binding-site, it approaches Asp-293 and interacts with its carboxylate group. In the case of (*S*)-HB, the interaction with Asp-293 may yield a much higher 3′(*S*)-hydroxylation activity as compared with the interaction with Glu-300, favoring 3′(*R*)-hydroxylation.

Even after a HB molecule sticks to the hydrophobic binding-site, the active-site cavity still has space sufficient for the interaction of another HB molecule with the carboxylate group of Glu-300, whereas the HB molecule stuck to the hydrophobic binding-site may interfere with approaching of another HB molecule to Asp-293. The replacement of phenylalanine residues at positions 100 and 476 may change the mode of interaction between HB and the hydrophobic binding-site, causing substantial changes in K_m or V_{max} values in the kinetic study. Particularly, the substitution of Phe-476 by alanine may make it impossible for the hydrophobic binding-site to capture (*S*)-HB, increasing the possibility of (*S*)-HB to approach Asp-293, resulting in a marked elevation of 3′(*S*)-OH-(*S*)-HB-forming activity.

As described before, the motivation of the current study was to determine the mechanism that caused different metabolite diastereoselectivity in BF 1″-hydroxylation between CYP2D6 and CYP2C19. In the current study, none of the substitution of the residues of CYP2C19 examined changed metabolite diastereoselectivity (3′*R* < 3′*S*, Fig. 1) in the enantiomeric HB 3′-hydroxylation. To our surprise, the diastereoselectivity as well as the total activity in BF 1″-hydroxylation were almost the same between CYP2C19 wild-type and CYP2C19-F476A (unpublished data). Therefore, Phe-476, which is a key residue in the reversal of the substrate enantioselectivity and the elevation of the total activity of HB 3′-hydroxylation, is not involved in BF 1″-hydroxylation by CYP2C19. Further studies are necessary to determine the mechanism causing the current results.

In summary, we examined the roles of amino acid residues such as Phe-100, Phe-114, Asp-293, Glu-300, and Phe-476 of CYP2C19 in stereoselective HB 3′-hydroxylation. CYP2C19 wild-type exerted substrate enantioselectivity of (*R*)-HB > (*S*)-HB and metabolite diastereoselectivity of 3′*R* < 3′*S* in 3′-hydroxylation of HB enantiomers. The substitution of Asp-293 by alanine failed to yield a functional P450 peak in the reduced CO-difference spectrum. Replacement of Glu-300 with aspartic acid did not markedly change the enzymatic functions, that with glutamine decreased the enzymatic activity, and that with valine tended to reverse the substrate enantioselectivity. A similar but much more pronounced reversal of the substrate enantioselectivity was caused by the replacement of Phe-476 with alanine, whereas the substitution of Phe-100 and Phe-114 with alanine did not produce such a marked change. These results indicate that Glu-300 and Phe-476 are important in stereoselective oxidation of HB enantiomers by CYP2C19.

ACKNOWLEDGMENTS

The authors appreciate the late Dr. Satoshi Toki, Fukuoka University, for his kind advice and a generous gift of HB enantiomers. The authors also thank Dr. Joyce A. Goldstein, National Institute of Environmental Health Sciences, for her generous gift of a plasmid, into which the cDNA encoding CYP2C19 wild-type was constructed.

LITERATURE CITED

1. Rendic S, Di Carlo FJ. Human cytochrome P450 enzymes: a status report summarizing their reactions, substrates, inducers and inhibitors. Drug Metab Rev 1997;29:413–580.
2. Parkinson A, Mudra DR, Johnson C, Dwyer A, Carroll M. The effects of gender, age, ethnicity, and liver cirrhosis on cytochrome P450 enzyme activity in human liver microsomes and inducibility in cultured human hepatocytes. Toxicol Appl Pharmacol 2004;199:193–209.
3. Evans WE, Relling MV. Pharmacogenomics: translating functional genomics into rational therapeutics. Science 1999;286:487–491.
4. Ingelman-Sundberg M. Pharmacogenetics of cytochrome P450 and its applications in drug therapy: the past, present and future. Trends Pharmacol Sci 2004;25:193–200.
5. Goldstein JA, Faletto MB, Romkes-Sparks M, Sullivan T, Kitareewan S, Raucy JL, Lasker JM, Ghanayem BI. Evidence that CYP2C19 is the major (S)-mephenytoin 4′-hydroxylase in humans. Biochemistry 1994;33:1743–1752.
6. Kubota T, Chiba K, Ishizaki T. Genotyping of S-mephenytoin 4′-hydroxylation in an extended Japanese population. Clin Pharmacol Ther 1996;60:661–666.
7. Goldstein JA. Clinical relevance of genetic polymorphisms in the human CYP2C subfamily. Br J Clin Pharmacol 2001;52:349–355.
8. Desta Z, Zhao X, Shin J-G, Flockhart DA. Clinical significance of the cytochrome P450 2C19 genetic polymorphism. Clin Pharmacokinet 2002;41:913–958.
9. Adedoyin A, Prakash C, O'Shea D, Blair IA, Wilkinson GR. Stereoselective disposition of hexobarbital and its metabolites: relationship to the S-mephenytoin polymorphism in Caucasian and Chinese subjects. Pharmacogenetics 1994;4:27–38.
10. Yasumori T, Murayama N, Yamazoe Y, Kato R. Polymorphism in hydroxylation of mephenytoin and hexobarbital stereosomers in relation to hepatic P-450 huamn-2. Clin Pharmacol Ther 1990;47:313–322.
11. Yasumori T, Yamazoe Y, Kato R. Cytochrome P-450 human-2 (P-450IIC9) in mephenytoin hydroxylation polymorphism in human livers: differences in substrate and stereoselectivities among microheterogeneous P-450IIC species expressed in yeasts. J Biochem 1991;109:711–717.
12. Narimatsu S, Takemi C, Tsuzuki D, Kataoka H, Yamamoto S, Shiinada N, Suzuki S, Satoh T, Meyer UA, Gonzalez FJ. Stereoselective metabolism of bufuralol racemate and enantiomers in human liver microsomes. J Pharmacol Exp Ther 2002;303:172–178.
13. Masuda K, Tamagake K, Katsu T, Torigoe F, Saito K, Hanioka N, Yamano S, Yamamoto S, Narimatsu S. The roles of phenylalanine at position 120 and glutamic acid at position 222 in the oxidation of chiral substrates by cytochrome P450 2D6. Chirality 2006;18:167–176.
14. Masuda K, Tamagake K, Okuda Y, Torigoe F, Tsuzuki D, Isobe T, Hichiya H, Hanioka N, Yamamoto S, Narimatsu S. Change in enantioselectivity in bufuralol 1″-hydroxylation by the substitution of phenylalanine-120 by alanine in cytochrome P450 2D6. Chirality 2005;17:37–43.
15. Williams PA, Cosme J, Ward A, Angove HC, Vinkovic DM, Jhoti H. Crystal structure of human cytochrome P450 2C9 with bound warfarin. Nature 2003;424:464–468.
16. Rowland P, Blaney FE, Smyth MG, Jones JJ, Leydon VR, Oxbrow AK, Lewis CJ, Tennant MG, Modi S, Eggleston DS, Chenery RJ, Bridges

AM. Crystal structure of human cytochrome P450 2D6. J Biol Chem 2006;281:7614–7622.

17. Ellis SW, Hayhurst GP, Smith G, Lightfoot T, Wong MMS, Simula AP, Ackland MJ, Sternberg MJE, Lennard MS, Tucker GT, Wolf CR. Evidence that aspartic acid 301 is a critical substrate-contact residue in the active site of cytochrome P450 2D6. J Biol Chem 1995;270: 29055–29058.
18. Hanna IH, Kim MS, Guengerich FP. Heterologous expression of cytochrome P450 2D6 mutants, electron transfer, and catalysis of bufuralol hydroxylation: The role of aspartate 301 in structure integrity. Arch Biochem Biophys 2001;393:255–261.
19. Melet A, Assrir N, Jean P, Lopez-Garcia MP, Marques-Soares C, Jaouen M, Dansette PN, Sari M-A, Mansuy D. Substrate selectivity of human cytochrome P450 2C9: importance of residues 476, 365, and 114 in recognition of diclofenac and sulfaphenazole and in mechanism-based inactivation by tienilic acid. Arch Biochem Biophys 2003;409:80–91.
20. Zanger UM, Raimundo S, Eichelbaum M. Cytochrome P450 2D6: overview and update on pharmacology, genetics, biochemistry. Naunyn-Schmiedeberg's Arch Pharmacol 2004;369:23–37.
21. Romanos MA, Scorer CA, Clare JJ. Foreign gene expression in yeast: a review. Yeast 1992;8:423–488.
22. Wan J, Imaoka S, Chow T, Hiroi T, Yabusaki Y, Funae Y. Expression of four rat CYP2D isoforms in *Saccharomyces cerevisiae* and their catalytic specificity. Arch Biochem Biophys 1997;348:383–390.
23. Hichiya H, Takemi C, Tsuzuki D, Yamamoto S, Asaoka K, Suzuki S, Satoh T, Shinoda S, Kataoka H, Narimatsu S. Complementary DNA cloning and characterization of cytochrome P450 2D29 from Japanese monkey liver. Biochem Pharmacol 2002;64:1101–1110.
24. Omura T, Sato R. The carbon monoxide-binding pigment of liver microsomes. I. Evidence for its hemoprotein nature. J Biol Chem 1964;239:2370–2378.
25. Tsuzuki D, Takemi C, Yamamoto S, Tamagake K, Imaoka S, Funae Y, Kataoka H, Shinoda S, Narimatsu S. Functional evaluation of cytochrome P450 2D6 with Gly42Arg substitution expressed in *Saccharomyces cerevisiae*. Pharmacogenetics 2001;11:709–718.
26. Takenoshita R, Toki S. New aspects of hexobarbital metabolism: Stereoselective metabolism, new metabolic pathway via GSH conjugation, and 3-hydroxyhexobarbital dehydrogenases. Yakugaku Zasshi (J Pharm Soc Jpn) 2004;124:858–871. (in Japanese).
27. Miyano K, Fuji Y, Toki S. Stereoselective hydroxylation of hexobarbital enntiomers by rat liver microsomes. Drug Metab Dispos 1984;8: 104–109.

Available online at www.sciencedirect.com
ScienceDirect
Biochemical and Biophysical Research Communications 357 (2007) 1100–1106
BBRC
www.elsevier.com/locate/ybbrc

Search of type 2 diabetes susceptibility gene on chromosome 20q

F. Takeuchi [a,1], K. Yanai [b,1], H. Inomata [b], N. Kuzuya [c], H. Kajio [c], S. Honjo [c], N. Takeda [d], Y. Kaburagi [e], K. Yasuda [e], S. Shirasawa [f], T. Sasazuki [g], N. Kato [b,*]

[a] *Department of Medical Ecology and Informatics, Research Institute, International Medical Center of Japan, Tokyo, Japan*
[b] *Department of Gene Diagnostics and Therapeutics, Research Institute, International Medical Center of Japan, 1-21-1 Toyama, Shinjuku-ku, Tokyo 162-8655, Japan*
[c] *Division of Metabolic Diseases, The Hospital, International Medical Center of Japan, Tokyo, Japan*
[d] *Division of Ophthalmology, The Hospital, International Medical Center of Japan, Tokyo, Japan*
[e] *Department of Metabolic Disorder, Research Institute, International Medical Center of Japan, Tokyo, Japan*
[f] *Department of Pathology, Research Institute, International Medical Center of Japan, Tokyo, Japan*
[g] *President, International Medical Center of Japan, Tokyo, Japan*

Received 31 March 2007
Available online 19 April 2007

Abstract

Significant evidence of linkage to type 2 diabetes (T2D) has been shown in a relatively broad region on chromosome 20q, where the hepatocyte nuclear factor-4α (*HNF4A*) has been noted as a positional candidate. To systematically evaluate genetic susceptibility to T2D in the relevant region, we examined the disease association by using 1145 SNPs in two-step screening in the Japanese population. The marker screening enabled us to identify significant disease association in the lipopolysaccharide binding protein (*LBP*) but not in the *HNF4A* locus. In a 17.7-Mb interval screened, the strongest association was identified for a SNP, rs2232592, located in the intron of *LBP*, with an estimated odds ratio of 1.73 (95% CI 1.30–2.31) ($P = 0.0002$) in the whole study panel involving 675 case and 474 control subjects. Our data suggest that the *LBP* gene may confer genetic susceptibility to T2D and this warrants further replication study.
© 2007 Elsevier Inc. All rights reserved.

Keywords: Diabetes; Genetics; Association; SNP; Japanese; Susceptibility; Hepatocyte nuclear factor-4α; Lipopolysaccharide binding protein

On chromosome 20q, suggestive evidence of linkage to type 2 diabetes has been repeatedly documented by genome-wide screening in several ethnic groups including the Japanese [1], Ashkenazi Jews [2], and Finn [3]. Peaks of linkage have been mapped to a relatively broad region (10–20 Mb) and some studies have indicated the presence of more than one diabetes susceptibility genes on 20q [3]. Permutt et al. [4] performed SNP-based screening of diabetes susceptibility genes with 91 SNPs in their target region spanning a LOD-1 interval (7.3 Mb in size) around D20S107. The authors reported that in the Ashkenazi Jewish population, borderline association ($P = 0.035$) with type 2 diabetes was detected at a single SNP, rs2664537. Independently, Silander et al. [5] performed SNP-based screening with 291 SNPs at 20q13.12–20q13.13 (6.7 Mb in size), where they had found a LOD score peak of 2.48 with a LOD-1 interval flanked by markers D20S861 and D20897 in the Finnish population. The strongest association with type 2 diabetes was detected at a SNP, rs2144908, in the P2 promoter region of the hepatocyte nuclear factor-4α (*HNF4A*) gene ($P = 0.01$, odds ratio 1.33). In parallel and almost simultaneously, the disease associations in the *HNF4A* locus were reported in the Ashkenazi Jewish families ($P = 0.0028$) [6] and later replicated in the UK population ($P = 0.02$) where there is no evidence of linkage to 20q [7]. Notably, in both the Finnish and Ashkenazi Jewish pedigrees used for genome-wide screening [2,3], most of the linkage signal on 20q appeared to be accounted for by the assumed risk allele of *HNF4A*.

* Corresponding author. Fax: +81 3 3202 7364.
E-mail address: nokato@ri.imcj.go.jp (N. Kato).
[1] These authors equally contributed to this work.

0006-291X/$ - see front matter © 2007 Elsevier Inc. All rights reserved.
doi:10.1016/j.bbrc.2007.04.063

To systematically evaluate genetic susceptibility to type 2 diabetes in the relevant region, we performed an extensive 'candidate' region approach on 20q where linkage to type 2 diabetes had been identified by genome-wide screening in the Japanese [1].

Materials and methods

Study population

Participants were recruited from the patients and their spouses who came regularly to the outpatient clinic of the Hospital of International Medical Center of Japan in Tokyo and the Hiranuma Clinic in Yokohama, both of which are located in the metropolitan area of Japan. The diagnosis of type 2 diabetes was based on the criteria of the World Health Organization. The patients with secondary diabetic disorders and maturity-onset of diabetes of the young were excluded. The normal control subjects were selected according to the following criteria: no past history of urinary glucose or glucose intolerance, an HbA_{1c} level <5.6% or a normal glucose (75 g) tolerance test, and age >60 years. Thus, a total of 675 cases and 474 controls were enrolled in the present study. All study subjects were unrelated, and they gave written consent for participation after being informed of the purpose of the study. The study protocol was approved by the Ethics Committee of International Medical Center of Japan.

Marker genotyping

The SNPs for genotyping were initially selected from the TaqMan® SNP Genotyping Assays (Applied Biosystems) in the candidate region for type 2 diabetes on 20q. We focused on the chromosome 20q region spanning a 17.7-Mb interval (from D20S195 to D20S196), which corresponded to a LOD-1 interval from the previous study in the Japanese [1]. While some were excluded due to a low minor allele frequency (MAF) in the Japanese, i.e., <0.05, a consecutive set of the TaqMan® Assays was used for the screening of diabetes susceptibility gene(s) on 20q. Also, in several regions where appropriate SNPs were unavailable from the TaqMan® Assays, we sought polymorphic markers from the dbSNP or JSNP (Japanese SNP) databases alternatively. Two-step screening was performed as follows. First, all the aforementioned SNPs were genotyped in a screening panel comprising 489 cases and 285 controls (Table 1). Second, after evaluation of the statistical significance by use of two models (independence on $[2 \times 3]$ contingency table for genotype distributions and independence on $[2 \times 2]$ contingency table for allele frequencies), SNPs that showed significant ($P < 0.01$) differences in either of the models were further examined in a combined panel involving an additional panel of 186 cases and 189 controls plus the screening panel. Moreover, not to leave the gaps within 10 kb from the SNPs that showed modestly significant ($P < 0.05$) association in the initial screening, we genotyped additional SNPs when applicable. A total of 1145 SNPs with MAF $\geqslant 0.05$ were genotyped in a 17.7-Mb region on 20q (an adjacent marker interval was 15.5 ± 0.5 kb). This set of SNPs covered 265 genes that were annotated in the relevant chromosomal region (NCBI Build 34). The arbitrary threshold of statistical significance in the combined panel was set to be $P < 0.01$ in either of two models.

In the *HNF4A* region, we genotyped a number of SNPs including those that had previously shown significant association with type 2 diabetes (rs1884614, rs2144908, and rs3818247) in the Finnish and Ashkenazi Jewish populations.

Statistical analysis

Association analysis. The SNPs were tested individually for the statistical significance of disease association with the χ^2-test statistic for genotype distributions and allele frequencies. SNPs' genotype departures from Hardy–Weinberg equilibrium (HWE) were tested using a χ^2-test with 1 degree of freedom.

The extent of linkage disequilibrium (LD) was measured in terms of an LD coefficient r^2 before the analysis of haplotype structure. By categorizing any pair of SNPs having $r^2 \geqslant 0.6$ into the same LD group, we defined LD blocks along the chromosomal region studied. Within each LD block, the frequencies of haplotypes were inferred from genotype data by the SNPHAP software [8] for the case and control groups, respectively. This restriction of SNPs to those constituting individual LD blocks could enhance the power to detect a disease locus [9]. Haplotype class counts for the separate case and control samples were then calculated as twice the number of individuals multiplied by the estimated haplotype frequencies, where haplotypes with frequencies less than 1% were neglected.

Because a significant association was detected around the lipopolysaccharide binding protein (*LBP*) gene in the initial screening, LD relations of SNPs were further examined in detail as previously reported [9].

Calculation of false discovery rate. To account for multiple testing of 1145 SNPs, we evaluated the false discovery rate (FDR), a practical and powerful approach to multiple testing [10], at *P*-values observed for individual genetic markers. The FDR is determined from the observed *P*-value distribution to provide a measure of the expected proportion of false positives among the data. The FDR differs from a *P*-value and higher values can be tolerated for FDRs than for *P*-values in some contexts.

Results

A total of 675 diabetic patients and 474 control subjects were enrolled in the present study. As type 2 diabetes was thought to be a late-onset disease, we set a criterion of age >60 years to minimize the risk of selecting control subjects who would become diabetic in the later age of life. Consequently, the present age in the control group was significantly older than that in the case group (Table 1). Although we did not have different selection criteria between the screening and additional panels, case subjects showed an earlier age of onset, higher values of maximum body mass index (BMI), and the higher incidence of diabetic complications in the screening panel than in the additional panel. This may be because we began SNP genotyping in the screening panel involving diabetic patients who had visited the outpatient clinic rather frequently (and who turned out to be relatively severely affected) and in the meanwhile we continued to recruit case subjects for the additional panel.

Association study

Overall success rate and accuracy of the genotyping assay exceeded 95% and 99.9%, respectively. For some instances (less than 5%), where genotyping data were not clearly distinguished in the scatter plot of the TaqMan® Assays or were not consistent with HWE, we sought alternative SNPs for the replacement. After the placement of additional SNP markers in the regions where suggestive association ($P < 0.05$) was detected in the initial SNP marker set (969 SNPs), among 1133 SNPs we found 44 SNPs to be significantly ($P < 0.01$ in either genotype distribution or allele frequency test) associated with type 2 diabetes in the initial screening (Supplementary Figure S1A). These 44 SNPs and 12 other SNPs that were located in the regions

Table 1
Clinical characteristics of participants

Variables	Case group			Control group		
	Combined panel	Screening panel	Additional panel	Combined panel	Screening panel	Additional panel
Number of subjects [female/male]	675 [277/398]	489 [201/288]	186 [76/110]	474 [276/198]	285 [165/120]	189 [111/78]
Present age (yr)	65.2 ± 10.9	64.7 ± 11.1	66.4 ± 10.2	70.7 ± 7.1	71.7 ± 7.2	69.1 ± 6.7†
Age of onset (yr)	50.4 ± 12.3	49.6 ± 12.0	52.3 ± 12.8*	—	—	—
Current body mass index (kg/m^2)	23.5 ± 3.6	23.7 ± 3.8	22.9 ± 3.2*	22.6 ± 3.3	22.5 ± 3.3	22.6 ± 3.2
Maximal body mass index (kg/m^2)	27.1 ± 4.2	27.4 ± 4.3	26.2 ± 3.7†	24.4 ± 3.3	24.7 ± 3.4	24.1 ± 3.2
Family history of diabetes (%)	57.2	59.0	52.5	11.3	9.2	14.3
Alcohol drinking						
None (%)	53.0	53.9	51.1	73.2	74.5	71.4
Previous drinker (%)	6.3	6.5	5.9	0.6	1.1	0
Current drinker (%)	40.7	38.1	43.0	26.1	24.5	28.6
Smoking						
None (%)	55.3	54.5	57.0	76.7	75.5	78.3
Previous smoker (%)	20.3	20.5	19.9	4.7	7.2	1.1
Current smoker (%)	24.4	25.0	23.1	18.6	17.3	20.6
Blood chemistry						
HbA1c (%)	7.49 ± 1.72	7.55 ± 1.77	7.33 ± 1.58	5.04 ± 0.38	5.04 ± 0.39	5.03 ± 0.37
Fasting plasma glucose (mg/dl)	153.1 ± 52.3	154.5 ± 52.2	149.5 ± 52.5	96.9 ± 12.6	95.6 ± 13.6	98.5 ± 10.9*
Serum total cholesterol (mg/dl)	192.7 ± 32.7	192.6 ± 33.7	192.7 ± 30.4	204.2 ± 31.1	203.3 ± 32.1	205.4 ± 29.7
Serum triglyceride (mg/dl)	136.8 ± 84.7	140.3 ± 89.7	128.8 ± 71.5	105.8 ± 56.9	109.5 ± 59.4	100.5 ± 52.8
Serum HDL cholesterol, mg/dl	51.0 ± 15.3	50.1 ± 15.1	53.0 ± 15.5*	64.9 ± 18.3	62.1 ± 17.9	68.9 ± 18.1†
Treatment of diabetes						
Diet therapy (%)	14.4	14.1	15.2	—	—	—
Oral hypoglycemic agents (OHA) (%)	65.0	64.3	66.8	—	—	—
Insulin therapy (%)	12.2	13.5	8.7	—	—	—
OHA+insulin therapy (%)	8.3	8.0	9.2	—	—	—
Prevalence of diabetic complications						
Neuropathy (%)	31.7	34.7	23.3*	—	—	—
Retinopathy (%)	32.6	34.1	28.6	—	—	—
Nephropathy (%)	30.2	31.5	26.9	—	—	—
All of triopathies (%)	15.7	17.6	10.5*	—	—	—
Prevalence of concomitant cardiovascular diseases						
Hypertension (%)	55.1	58.2	47.0*	32.6	33.6	31.2
Hyperlipidemia (%)	42.6	43.6	39.8	22.2	20.4	24.7
Ischemic heart disease (%)	15.8	15.4	16.7	—	—	—

All clinical assessments were performed using uniform standards. The current body mass index (BMI) was directly measured when blood samples were collected for DNA analysis. The age at onset of diabetes, maximum BMI, alcohol consumption, and habitual smoking were obtained from direct interviews by trained interviewers. The diagnosis of diabetic complications and concomitant cardiovascular diseases was validated by specialist doctors. Only the participants with thorough evaluation of diabetic complications or cardiovascular diseases were used for the calculation of the corresponding prevalence. Values are means ± SD.

ANOVA was performed between the screening panel and the additional panel for case and control groups, respectively.

* $P < 0.05$.

† $P < 0.001$.

of interest were further genotyped in the additional panel. Here, FDR was <0.1 for the most significant four SNPs (rs2232592, rs1739654, rs1105402, and rs11908089) among 1145 in the screening panel.

In most of the 56 SNPs tested, *P*-values for allele frequency and those for genotype distribution became almost unchanged or less significant when analyzing the data in the combined panel (Supplementary Figure S1B and S1C). Finally, we selected 10 SNPs which were (1) significant ($P < 0.01$ in either genotype distribution or allele frequency test) in the combined panel and (2) concordant in odds ratio tendency of allele frequency in the screening and additional panels (Table 2). We estimated type I error probability for the two-step screening to be 0.00456. Since we had adopted relatively generous criteria for screening of association signals, we evaluated FDR to account for multiple testing in the entire screening. FDR for 10 SNPs finally selected was 0.52. Still, of note is the fact that four out of 10 SNPs were located in the vicinity of *LBP* (colored red in Figure S1B).

We thus observed the strongest evidence for association in the *LBP* region (Fig. 1A) but not in the *HNF4A* region (Fig. 1B) in our studied population. Four SNPs spanning a 23-kb interval showed $P = 0.003$–0.0002 in *LBP* (Table 2). On the other hand, three SNPs previously reported [5,6]—two SNPs (rs1884614 and rs2144908) in the P2 promoter region and a SNP (rs3818247) in the intron of *HNF4A*—failed to show significant association in the combined panel, nor did eight other SNPs located in the *HNF4A* region.

Also, we examined disease association in five other regions, where significant *P*-values ($P < 0.01$) were detected with the genotype and/or allele frequencies being analyzed in the combined panel (Table 2). No strong evidence in favor of diabetes susceptibility genes existed in any of these regions.

We further performed haplotype analysis by defining LD blocks along the chromosomal region and a total of 200 LD blocks (which comprised more than 1 SNPs with MAF $\geqslant 0.05$) were constructed at the level of $r^2 \geqslant 0.6$. We found that only one LD block including rs13044736 showed *P*-value <0.01 (0.0045) for χ^2-test statistic on haplotypes, whereas the majority of LD blocks showed almost equivalent *P*-values for χ^2-test statistic on haplotypes and individual SNPs (data not shown). A minor haplotype involving two SNPs in the P2 promoter region of *HNF4A* (TG for rs1884614 and rs2144908) has been recently reported to be enriched from 1.4% in nondiabetic subjects to 4.4% in diabetic subjects in the Japanese [11]. However, this haplotype was not observed either in diabetic or nondiabetic subjects in our study (see Table 3).

Genetic analysis in the LBP gene

Three SNPs (rs1739654, rs1739639, and rs1780627) in *LBP* were used for the initial screening, while rs1739639 was not subjected for the further analysis due to its low MAF (0.03–0.04) in the Japanese population. We tested disease association with a total of eight SNPs including additional six SNPs within the *LBP* gene that consisted of 15 exons spanning 31.5-kb. We found four SNPs—rs2232578, rs1739654, rs2232592, and rs1780627—to be significantly ($P < 0.01$) associated with type 2 diabetes in the combined panel (Table 2). All significant SNPs belonged to the same cluster with close intra-cluster pairwise LD but there was no haplotype class showing more significant disease association than individual SNPs (see Supplementary Table S1).

Discussion

Based on the linkage results from the study in the Japanese [1], we have explored diabetes susceptibility genes in a 17.7-Mb region that contains 265 annotated genes. At the arbitrary threshold of $P < 0.01$, 3.9% of SNPs tested in the initial screening (44 out of 1133 SNPs) has turned out to be significant and we have attempted to validate them by increasing the study subjects. Among the 10 SNPs finally selected, in terms of statistical significance of disease association, best three SNPs were located in the *LBP* gene when we analyzed the data in the combined panel (Supplementary Figure S1B and S1C).

In the *LBP* region, there are two SNP clusters in complete LD, which partially overlap each other in the middle of the *LBP* gene (Supplementary Figure S2). Among best three SNPs that have shown significant association with type 2 diabetes, rs1739654 is located in the coding region (synonymous mutation) while rs2232578 and rs2232592 are in the 5′-region and intron of *LBP*, respectively. According to the LD plot and haplotype phylogeny (data not shown), diabetes risk determinants could be located anywhere within and in the close proximity of the *LBP* gene. Notably, when we have attempted stratified analysis for rs2232592, genetic risk attributable to *LBP* is pronounced in diabetic patients with the younger age of onset and/or those with the history of severer obesity (see Supplementary Figure S3).

LBP is an acute phase protein that strongly modulates the response to lipopolysaccharides (LPS) or endotoxins, which are a component of the surface of the outer membrane of Gram-negative bacteria. LBP is an important parameter for monitoring the acute phase and the ability of the host to react to LPS stimulation [12]. While detailed mechanisms of acute phase response to LPS have been investigated by studies *in vitro* and *in vivo* [13,14], no studies have reported a direct functional link between LPS (or inflammation induced by Gram-negative bacteria) and type 2 diabetes so far. One of the potential mechanisms linking LBP to glucose metabolism would be obesity, adipose tissue-derived molecules such as leptin, and inflammation, which, together, are hypothesized to underlie the 'obesity-diabetes connection' [15].

In view of high-resolution marker genotyping, we should consider statistical power and type I error probability, both

Table 2
Association analysis of genotype and allele frequency distributions for SNPs in the selected regions on chromosome 20q

SNP name[a]	Gene	Major(M)/minor(m) allele	Screening panel ($n = 774$)					Combined panel [screening + additional panel] ($n = 1149$)					
			Genotype			Allele		Genotype			Allele		
			Case MM/Mm/mm	Control MM/Mm/mm	*P*-value	MAF case/control	*P*-value	Case MM/Mm/mm	Control MM/Mm/mm	*P*-value	MAF case/control	*P*-value	OR (95%CI)[b]
In the LBP region													
rs1934915	Intergenic	A/G	339/117/19	169/105/13	0.001	0.16/0.23	0.002	453/178/31	293/163/22	0.030	0.18/0.22	0.036	0.80 (0.65–0.99)
rs1341020	Intergenic	G/C	435/38/0	254/30/3	0.042	0.04/0.06	0.048	—	—	—	—	—	—
rs1341022	BPI	C/G	175/212/88	112/142/32	0.026	0.41/0.36	0.061	—	—	—	—	—	—
rs2275954	BPI	A/G	160/212/103	77/144/65	0.138	0.44/0.48	0.139	212/314/136	136/229/110	0.377	0.44/0.47	0.156	0.89 (0.75–1.05)
rs2256754	BPI	A/G	140/213/118	85/142/55	0.186	0.48/0.45	0.261	188/311/154	140/237/92	0.281	0.47/0.45	0.239	1.11 (0.94–1.31)
rs1579101	BPI	C/T	148/209/111	70/147/68	0.089	0.46/0.50	0.175	—	—	—	—	—	—
rs1739635	Intergenic	G/A	142/211/116	86/143/58	0.290	0.47/0.45	0.425	—	—	—	—	—	—
rs2232578	LBP	A/G	291/165/17	212/70/3	0.0006	0.21/0.13	0.0002	420/218/22	346/118/9	0.003	0.20/0.14	0.0007	1.47 (1.18–1.85)
rs1739654	LBP	G/A	333/128/9	230/50/0	0.0006	0.16/0.09	0.0002	475/170/12	383/84/3	0.001	0.15/0.10	0.0003	1.64 (1.25–2.13)
rs2232592	LBP	G/A	350/118/6	247/38/1	0.0002	0.14/0.07	0.00006	501/152/8	407/66/4	0.0004	0.13/0.08	0.0002	1.73 (1.30–2.31)
rs2298266	LBP	C/T	310/139/24	170/97/19	0.223	0.20/0.24	0.077	433/193/33	309/143/24	0.961	0.20/0.20	0.808	0.97 (0.79–1.20)
rs2298267	LBP	G/A	160/228/78	93/124/67	0.065	0.41/0.45	0.109	215/ 317/119	155/218/96	0.619	0.43/0.44	0.609	0.96 (0.81–1.13)
rs3819023	LBP	A/G	430/44/0	256/30/1	0.377	0.05/0.06	0.418	596/65/0	427/48/2	0.247	0.05/0.05	0.569	0.90 (0.62–1.30)
rs1780627	LBP	C/T	313/147/12	221/64/2	0.004	0.18/0.12	0.001	453/191/16	364/109/5	0.011	0.17/0.12	0.003	1.43 (1.12–1.82)
rs1739640	LBP	C/T	342/122/11	227/58/2	0.044	0.15/0.11	0.016	484/165/14	375/97/4	0.039	0.15/0.11	0.014	1.37 (1.07–1.77)
rs4811789	Intergenic	T/C	162/202/109	96/123/61	0.912	0.44/0.44	0.807	—	—	—	—	—	—
rs1780634	Intergenic	C/T	297/152/23	181/88/17	0.776	0.21/0.21	0.870	—	—	—	—	—	—
rs752774	LOC388796	G/A	379/88/5	218/61/5	0.435	0.10/0.13	0.205	—	—	—	—	—	—
rs1303582	KIAA1219	G/A	384/83/6	218/62/5	0.297	0.10/0.13	0.119	—	—	—	—	—	—
In the HNF4A region													
rs1884614	P2 of HNF4A	C/T	145/231/95	91/146/49	0.586	0.45/0.43	0.439	200/324/134	154/239/83	0.443	0.45/0.43	0.247	1.10 (0.93–1.31)
rs2144908	P2 of HNF4A	G/A	143/232/97	91/144/50	0.592	0.45/0.43	0.379	198/324/137	153/239/84	0.396	0.45/0.43	0.215	1.11 (0.94–1.32)
rs3818247	HNF4A	T/G	177/229/66	103/152/29	0.228	0.38/0.37	0.622	249/321/89	175/250/50	0.234	0.38/0.37	0.621	1.04 (0.88–1.24)
Other loci showing suggestive evidence for association													
rs2297056	ELMO2	C/T	265/156/22	186/83/6	0.043	0.23/0.17	0.016	381/217/33	311/143/12	0.024	0.22/0.18	0.010	1.32 (1.07–1.64)
rs2257545	ELMO2	C/T	259/180/35	185/87/15	0.027	0.26/0.20	0.008	359/253/50	294/160/23	0.023	0.27/0.22	0.006	1.32 (1.08–1.61)
rs11908089	Intergenic	C/T	190/233/50	151/115/20	0.002	0.35/0.27	0.001	263/325/73	233/210/34	0.004	0.36/0.29	0.001	1.35 (1.12–1.61)
rs827934	Intergenic	G/T	98/240/133	85/140/60	0.008	0.54/0.46	0.002	154/320/185	137/231/105	0.029	0.52/0.47	0.007	1.25 (1.06–1.49)
rs752255	Intergenic	T/C	413/55/3	266/17/0	0.014	0.06/0.03	0.003	589/67/3	447/27/0	0.009	0.06/0.03	0.002	2.00 (1.28–3.14)
rs13044736	PREX1	A/G	358/104/12	190/92/3	0.004	0.14/0.17	0.050	492/156/14	311/156/8	0.002	0.14/0.18	0.006	0.73 (0.58–0.92)

All markers were initially characterized in the screening panel (which comprised 489 cases and 285 controls) and then selected markers were further characterized in the additional panel (which comprised 186 cases and 189 controls) (see Materials and methods). Results for the screening panel and the combined panel (i.e., screening plus additional panel) are displayed in the table. The data cells are denoted as blank "—" for the markers characterized in the screening panel alone. As for allele frequency distribution, *P*-values calculated by the χ^2-test were plotted for SNPs in the LBP and HNF4A regions in Fig. 1.

[a] Three SNPs selected in the HNF4A region were previously reported to show significant association with diabetes in the Finnish and Ashkenazi Jewish populations (Refs. [5,6]).

[b] Odds ratio (OR) was calculated for the minor allele in control subjects.

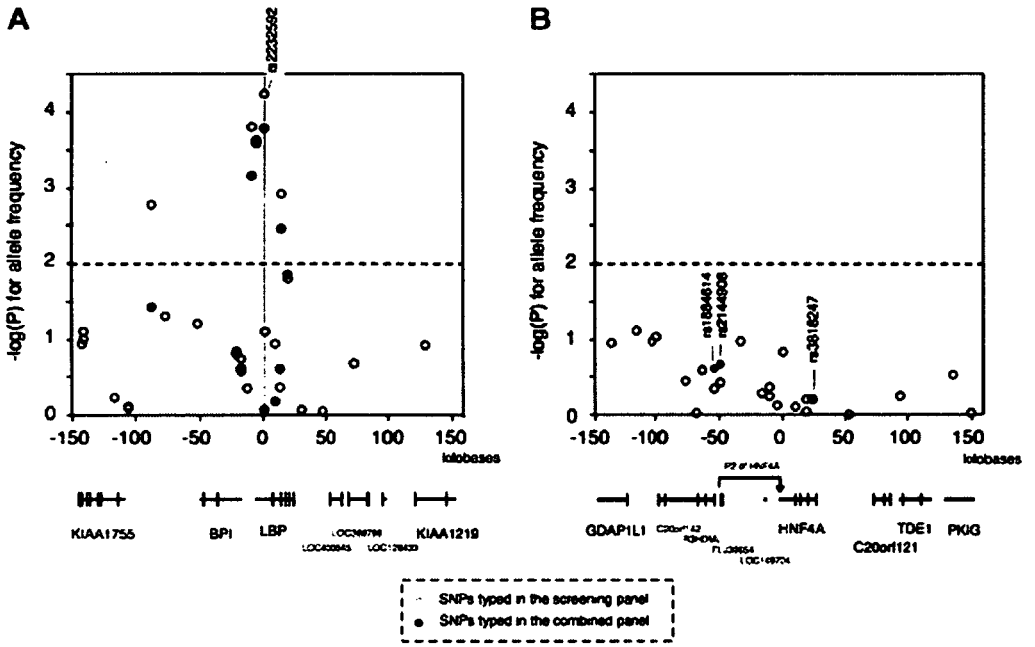

Fig. 1. Association of markers from the *LBP* and *HNF4A* regions with type 2 diabetes. Results for SNPs genotyped in the screening and combined panels are shown with open (O) and solid (●) circles, respectively. Horizontal dotted lines indicate the $-\log_{10}$ *P*-value = 2, i.e., $P = 0.01$. (A) $-\log_{10}$ *P*-values of the differences in allele frequencies between case and control subjects were plotted against physical distance as centered by the most significantly associated marker rs2232592 in *LBP*. At the bottom, partial exons of known and predicted genes are shown. (B) $-\log_{10}$ *P*-values of the differences in allele frequencies between case and control subjects were plotted against physical distance as centered by the translation initiation site of *HNF4A*. The location of the three SNPs that are associated with diabetes status in Finns and Ashkenazi Jews is labeled.

Table 3
Haplotypes estimated in the P2 promoter region of HNF4A locus

Class	Haplotype	Frequency of haplotype	
		Case	Control
1	CG	0.548	0.572
2	TA	0.450	0.426
3	CA	0.002	0.002
4	TG	—	—

Haplotypes were estimated for 2 SNPs (rs1884614 and rs2144908) in the P2 promoter region of HNF4A locus. See also Table 2 about genotype and allele frequencies of each SNP. For each haplotype, its frequency in the case and control groups is shown. A 'TG' haplotype was not observed in the combined panel (675 cases and 474 controls).

issues are brought up by our screening strategy. First, to address the issue of statistical power, we have performed simulation analysis by calculating the ratio of encountered times surpassing the cut-off level ($P < 0.01$) of association among 1000-times simulation data sets (data not shown). When we test SNPs assumably having the odds ratio of 1.7 (as in the case of rs2232592) for allele frequency comparison, we can expect the statistical power which represents the ratio of [true positives/(true positives + false negatives)] to be more than 80% assuming multiplicative or additive mode of inheritance, disease allele frequency between 0.2 and 0.8, and 10% prevalence. From the methodological point of view, however, we should bear in mind several limitations of the present study. When we consider the marker density (1 SNP per 15.5 kb on average) and random selection procedure without utilizing LD information, there is likely to be a certain amount of common variations not captured. Across the target chromosomal region of 20q, we have assessed the percentage of common variations that are covered by the SNPs genotyped in the present study. Approximately 71% (814 of 1145) of SNPs were shared with the HapMap database (Release 19), and 45% of the HapMap SNPs (with MAF $\geqslant 0.05$) from JPT is estimated to have a high r^2 (>0.8) to one of the shared SNPs. The remaining 29% (331 of 1145) of our SNPs not in HapMap have captured further information of variations. Second, to evaluate the type I error probability caused by multiple testing, we have calculated the FDR at *P*-values observed for individual genetic markers and we have found the lowest FDR of 0.14 for significant SNPs rs2232592 and rs1739654 in *LBP* when disease association is tested in the combined panel. Thus, our results are worth following up even though far from definitive in the present study alone. The only way to identify definitive findings from false positives is to replicate the results in other studies.

Another important issue is the lack of evidence for disease association in the *HNF4A* region in our Japanese population (Fig. 1B and Tables 2 and 3). This does not refute the disease causality of the *HNF4A* gene by itself, which has been argued by a number of studies [5–7,11,16–20]. Assuming that the increase in type 2 diabetes risk with the rs2144908 genotype of *HNF4A* is ≈33% [5], >800 indi-

viduals are required in each group of cases and controls with 80% power at 5% type I error probability. It is therefore possible that the underpowered sample size results in the lack of evidence for association in the *HNF4A* region. It is also possible that diabetes susceptibility gene(s) differ among ethnic groups, since peaks of linkage have been mapped to a relatively broad region of chromosome 20q with partial overlapping.

In conclusion, we have identified the *LBP* gene as a most likely candidate for conferring genetic susceptibility to type 2 diabetes on chromosome 20q in the Japanese population. These findings warrant further replication study, but once replicated, the biological relevance of *LBP* will become an issue of great interest.

Acknowledgments

This work was supported by the grant from the Program for Promotion of Fundamental Studies in Health Sciences of Pharmaceuticals and Medical Devices Agency (PMDA) and that of the National Institute of Biomedical Innovation (NIBI). We thank Ms. Mika Higashida and Ms. Hisae Shiina, and Dr. Kei Fujimoto and Dr. Kanae Yasuda for their help in data and sample collection.

Appendix A. Supplementary data

Supplementary data associated with this article can be found, in the online version, at doi:10.1016/j.bbrc.2007.04.063.

References

[1] Y. Mori, S. Otabe, C. Dina, K. Yasuda, C. Populaire, C. Lecoeur, V. Vatin, E. Durand, K. Hara, T. Okada, K. Tobe, P. Boutin, T. Kadowaki, P. Froguel, Genome-wide search for type 2 diabetes in Japanese affected sib-pairs confirms susceptibility genes on 3q, 15q, and 20q and identifies two new candidate Loci on 7p and 11p, Diabetes 51 (2002) 1247–1255.

[2] M.A. Permutt, J.C. Wasson, B.K. Suarez, J. Lin, J. Thomas, J. Meyer, S. Lewitzky, J.S. Rennich, A. Parker, L. DuPrat, S. Maruti, S. Chayen, B. Glaser, A genome scan for type 2 diabetes susceptibility loci in a genetically isolated population, Diabetes 50 (2001) 681–685.

[3] S. Ghosh, R.M. Watanabe, E.R. Hauser, T. Valle, V.L. Magnuson, M.R. Erdos, C.D. Langefeld, J. Balow Jr., D.S. Ally, K. Kohtamaki, P. Chines, G. Birznieks, H.S. Kaleta, A. Musick, C. Te, J. Tannenbaum, W. Eldridge, S. Shapiro, C. Martin, A. Witt, A. So, J. Chang, B. Shurtleff, R. Porter, K. Kudelko, A. Unni, L. Segal, R. Sharaf, J. Blaschak-Harvan, J. Eriksson, T. Tenkula, G. Vidgren, C. Ehnholm, E. Tuomilehto-Wolf, W. Hagopian, T.A. Buchanan, J. Tuomilehto, R.N. Bergman, F.S. Collins, M. Boehnke, Type 2 diabetes: evidence for linkage on chromosome 20 in 716 Finnish affected sib pairs, Proc. Natl. Acad. Sci. USA 96 (1999) 2198–2203.

[4] M.A. Permutt, J. Wasson, L. Love-Gregory, J. Ma, G. Skolnick, B. Suarez, J. Lin, B. Glaser, Searching for type 2 diabetes genes on chromosome 20, Diabetes 51 (Suppl. 3) (2002) S308–S315.

[5] K. Silander, K.L. Mohlke, L.J. Scott, E.C. Peck, P. Hollstein, A.D. Skol, A.U. Jackson, P. Deloukas, S. Hunt, G. Stavrides, P.S. Chines, M.R. Erdos, N. Narisu, K.N. Conneely, C. Li, T.E. Fingerlin, S.K. Dhanjal, T.T. Valle, R.N. Bergman, J. Tuomilehto, R.M. Watanabe, M. Boehnke, F.S. Collins, Genetic variation near the hepatocyte nuclear factor-4 alpha gene predicts susceptibility to type 2 diabetes, Diabetes 53 (2004) 1141–1149.

[6] L.D. Love-Gregory, J. Wasson, J. Ma, C.H. Jin, B. Glaser, B.K. Suarez, M.A. Permutt, A common polymorphism in the upstream promoter region of the hepatocyte nuclear factor-4 alpha gene on chromosome 20q is associated with type 2 diabetes and appears to contribute to the evidence for linkage in an Ashkenazi Jewish population, Diabetes 53 (2004) 1134–1140.

[7] M.N. Weedon, K.R. Owen, B. Shields, G. Hitman, M. Walker, M.I. McCarthy, L.D. Love-Gregory, M.A. Permutt, A.T. Hattersley, T.M. Frayling, Common variants of the hepatocyte nuclear factor-4 alpha P2 promoter are associated with type 2 diabetes in the U.K. population, Diabetes 53 (2004) 3002–3006.

[8] D Clayton, SNPHAP—A program for estimating frequencies of large haplotypes of SNPs, Electronic-database is available from http://archimedes.well.ox.ac.uk/pise/snphap-simple.html.

[9] F. Takeuchi, K. Yanai, T. Morii, Y. Ishinaga, K. Taniguchi-Yanai, S. Nagano, N. Kato, Linkage disequilibrium grouping of SNPs reflecting haplotype phylogeny for efficient selection of tag SNPs, Genetics 170 (2005) 291–304.

[10] Y. Benjamini, Y. Hochberg, Controlling the false discovery rate: a practical and powerful approach to multiple testing, J. R. Stat. Soc. B 57 (1995) 289–300.

[11] K. Hara, M. Horikoshi, H. Kitazato, C. Ito, M. Noda, J. Ohashi, P. Froguel, K. Tokunaga, K. Tobe, R. Nagai, T. Kadowaki, Hepatocyte nuclear factor-4alpha P2 promoter haplotypes are associated with type 2 diabetes in the Japanese population, Diabetes 55 (2006) 1260–1264.

[12] R.R. Schumann, J. Zweigner, A novel acute-phase marker: lipopolysaccharide binding protein (LBP), Clin. Chem. Lab. Med. 37 (1999) 271–274.

[13] S.D. Wright, R.A. Ramos, P.S. Tobias, R.J. Ulevitch, J.C. Mathison, CD14, a receptor for complexes of lipopolysaccharide (LPS) and LPS binding protein, Science 249 (1990) 1431–1433.

[14] R.S. Jack, X. Fan, M. Bernheiden, G. Rune, M. Ehlers, A. Weber, G. Kirsch, R. Mentel, B. Furll, M. Freudenberg, G. Schmitz, F. Stelter, C. Schutt, Lipopolysaccharide binding protein is required to combat a murine gram-negative bacterial infection, Nature 389 (1997) 742–745.

[15] M.A. Lazar, How obesity causes diabetes: not a tall tale, Science 307 (2005) 373–375.

[16] S.K. Hansen, C.S. Rose, C. Glumer, T. Drivsholm, K. Borch-Johnsen, T. Jorgensen, O. Pedersen, T. Hansen, Variation near the hepatocyte nuclear factor (HNF)-4alpha gene associates with type 2 diabetes in the Danish population, Diabetologia 48 (2005) 452–458.

[17] W. Winckler, R.R. Graham, P.I. de Bakker, M. Sun, P. Almgren, T. Tuomi, D. Gaudet, T.J. Hudson, K.G. Ardlie, M.J. Daly, J.N. Hirschhorn, L. Groop, D. Altshuler, Association testing of variants in the hepatocyte nuclear factor 4alpha gene with risk of type 2 diabetes in 7,883 people, Diabetes 54 (2005) 886–892.

[18] A.M. Bagwell, J.L. Bento, J.C. Mychaleckyj, B.I. Freedman, C.D. Langefeld, D.W. Bowden, Genetic analysis of HNF4A polymorphisms in Caucasian-American type 2 diabetes, Diabetes 54 (2005) 1185–1190.

[19] Y.L. Muller, A.M. Infante, R.L. Hanson, L. Love-Gregory, W. Knowler, C. Bogardus, L.J. Baier, Variants in hepatocyte nuclear factor 4alpha are modestly associated with type 2 diabetes in Pima Indians, Diabetes 54 (2005) 3035–3039.

[20] Q. Zhu, K. Yamagata, A. Miura, N. Shihara, Y. Horikawa, J. Takeda, J. Miyagawa, Y. Matsuzawa, T130I mutation in HNF-4alpha gene is a loss-of-function mutation in hepatocytes and is associated with late-onset Type 2 diabetes mellitus in Japanese subjects, Diabetologia 46 (2003) 567–573.

© 2008 The Authors
Journal compilation © 2008 Nordic Pharmacological Society. Basic & Clinical Pharmacology & Toxicology, 102, 388–393
Doi: 10.1111/j.1742-7843.2008.00222.x

Influence of *CYP2C19*18* and *CYP2C19*19* Alleles on Omeprazole 5-Hydroxylation: *In vitro* Functional Analysis of Recombinant Enzymes Expressed in *Saccharomyces cerevisiae*

Nobumitsu Hanioka[1], Yumi Tsuneto[1], Yoshiro Saito[2], Keiko Maekawa[2], Jun-ichi Sawada[2] and Shizuo Narimatsu[1]

[1]Graduate School of Medicine, Dentistry and Pharmaceutical Sciences, Okayama University, Tsushima-naka, Okayama, Japan, [2]Division of Biochemistry and Immunochemistry, National Institute of Health Sciences, Kamiyoga, Setagaya-ku, Tokyo, Japan

(Received August 24, 2007; Accepted October 5, 2007)

Abstract: Omeprazole is one of the most widely used proton pump inhibitors for the treatment of gastric acid-related disorders. The major metabolic pathway of omeprazole is 5-hydroxylation, which is catalysed by CYP2C19. In this study, the effect of *CYP2C19*18* and *CYP2C19*19* alleles on omeprazole 5-hydroxylation was studied using recombinant CYP2C19 enzymes of wild-type (CYP2C19.1B having Ile331Val) and variants (CYP2C19.18 having Arg329His/Ile331Val and CYP2C19.19 Ser51Gly/Ile331Val) expressed in yeast cells. The K_m value for omeprazole 5-hydroxylation of CYP2C19.1B was 1.46 μM. The K_m value of CYP2C19.19 was significantly higher (1.5-fold) than that of CYP2C19.1B. V_{max} and V_{max}/K_m values for omeprazole 5-hydroxylation of CYP2C19.1B on the basis of cytochrome P450 protein level were 8.09 pmol/min./pmol CYP and 5.45 μl/min./pmol CYP, respectively. The V_{max} value of CYP2C19.19 was significantly higher (1.8-fold) than that of CYP2C19.1B, whereas the V_{max}/K_m value was comparable to that of CYP2C19.1B. In contrast, K_m, V_{max} and V_{max}/K_m values of CYP2C19.18 were similar to those of CYP2C19.1B. These results suggest that *CYP2C19*19* allele decreases the affinity between CYP2C19 enzyme and the substrate in omeprazole metabolism.

Omeprazole (fig. 1), a proton pump inhibitor, has been widely used for many years as an acid inhibitory agent for the treatment of gastric acid hypersecretion disorders [1,2]. Omeprazole has been shown to be extensively metabolized in the liver by the cytochrome P450 (CYP) enzyme system to the primary metabolite of 5-hydroxyomeprazole (fig. 1), and omeprazole sulfone [3,4]. The formation of 5-hydroxyomeprazole as the major metabolite is mainly mediated by CYP2C19, whereas the formation of omeprazole sulfone as the minor metabolite is by CYP3A4 [5–8].

The pharmacokinetics and pharmacodynamics of omeprazole significantly depend on CYP2C19 phenotype or genotype status, and individuals can be divided into an extensive metabolizer (EM) group and a poor metabolizer (PM) group [9–11]. It has been reported that the higher plasma concentration of omeprazole in PMs shows higher effectiveness in anti-*Helicobacter pylori* therapy, higher gastric pH and possibly higher stability of antimicrobials in clinical situations [12]. The area under the plasma concentration time curve of oral omeprazole in PMs of CYP2C19 is significantly larger than that of EMs [11,13–15]. Furthermore, ethnic differences have been reported in the PM frequency of CYP2C19 enzyme: 2–5% in Caucasian populations, 2–5% in Black populations and 13–25% in Oriental populations [11,16].

Various mutations of the *CYP2C19* gene have been identified from ethnically different populations (http://www.imm.ki.se/CYPalleles/cyp2c19.htm). The PM-related *CYP2C19* polymorphism of Oriental populations can be explained by the combination of two-point mutations, *CYP2C19*2* (681G>A, splicing defect) of exon 5 and *CYP2C19*3* (636G>A, Trp212Stop) of exon 4 [9,10]. In Caucasian populations, additionally deficient *CYP2C19* alleles have been subsequently found, although only 2–5% of populations show the PM phenotype [17–22]. Recently, we also identified two alleles (haplotypes), termed *CYP2C19*18* (986G>A/991A>G, Arg329His/Ile331Val) and *CYP2C19*19* (151A>G/991A>G, Ser51Gly/Ile331Val), in a Japanese population at a frequency of 0.2–0.3%, and found that *CYP2C19*19* allele alters the metabolic ability towards *S*-mephenytoin of CYP2C19 enzyme [23,24].

The purpose of this study was to investigate whether genetic polymorphisms of *CYP2C19*18* and *CYP2C19*19* affect the metabolism of omeprazole. To achieve this, CYP2C19 enzymes of wild-type (CYP2C19.1B) and variants (CYP2C19.18 and CYP2C19.19) were heterologously expressed in yeast cells, and the kinetics of omeprazole 5-hydroxylation were determined.

Materials and Methods

Materials. CYP2C19*1A cDNA cloned into pBluescript-SK(±) vector (pBluescript/CYP2C19*1A) was kindly provided by Dr. Joyce A. Goldstein (National Institute of Environmental Health Sciences, Research Triangle Park, NC, USA). KOD-plus DNA

Nobumitsu Hanioka and Yumi Tsuneto contributed equally to this article.

Author for correspondence: Shizuo Narimatsu, Graduate School of Medicine, Dentistry and Pharmaceutical Sciences, Okayama University, 1-1-1 Tsushima-naka, Okayama 700-8530, Japan (fax +81-86-251-7942, e-mail shizuo@pharm.okayama-u.ac.jp).

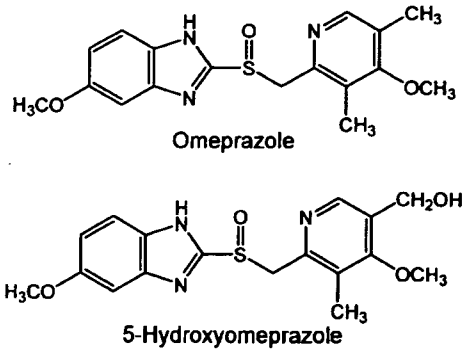

Fig. 1. Chemical structures of omeprazole and 5-hydroxyomeprazole.

polymerase was purchased from Toyobo (Osaka, Japan); *Hin*dIII was from Takara Bio (Ohtsu, Japan); BigDye terminator cycle sequencing reaction kit v3.1 was from Applied Biosystems (Foster City, CA, USA); pcDNA3.1(+) vector was from Invitrogen (Carlsbad, CA, USA); and QuikChange site-directed mutagenesis kit was from Stratagene (La Jolla, CA, USA). The expression vector pGYR1, which has a glyceraldehyde-3-phosphate dehydrogenase (GAPDH) promoter and includes the yeast NADPH-P450 reductase gene [25], was kindly provided by Dr. Yoshihiko Funae (Osaka City University, Osaka, Japan). Yeast nitrogen base was purchased from BD Diagnostics (Franklin Lakes, NJ, USA); omeprazole and lansoprazole were from Sigma-Aldrich (St. Louis, MO, USA). 5-Hydroxyomeprazole was supplied by AstraZeneca R&D Mölndal (Mölndal, Sweden). $NADP^+$, glucose 6-phosphate and glucose 6-phosphate dehydrogenase were obtained from Oriental Yeast (Tokyo, Japan); rabbit anti-human CYP2C19 antibody was from BD Biosciences (San Jose, CA, USA); peroxidase-conjugated goat anti-rabbit immunoglobulin was from Zymed Laboratories (South San Francisco, CA, USA); and enhanced chemiluminescence-plus reagents were from GE Healthcare Bio-Sciences (Little Chalfont, UK). All other chemicals and reagents were of the highest quality commercially available.

Construction of CYP2C19 plasmids. CYP2C19 expression plasmids of wild-type (pGYR1/CYP2C19*1C) and variants (pGYR1/CYP2C19*18 and pGYR1/CYP2C19*19) were constructed as described previously [24]. Briefly, CYP2C19*1A cDNA was amplified by PCR from pBluescript/CYP2C19*1A as a template using the forward primer 5′-CCCAAGCTTAA*AAAA*ATGGATCCTTTT-GTGGTCC-3′ and the reverse primer 5′-GGAAAGCTTAGGAG-CAGCCAGACCATCTGT-3′. *Hin*dIII sites (marked with solid lines) were introduced to the 5′-end of the start codon and the 3′-end of the stop codon to facilitate subcloning into pGYR1. A yeast consensus sequence (marked in italics) was also introduced upstream of the start codon to achieve a high expression of protein in yeast cells [26]. The PCR product was digested with *Hin*dIII and ligated into the same restriction enzyme site of pcDNA3.1(+), resulting in pcDNA3.1/CYP2C19*1A. The pcDNA3.1/CYP2C19*1A plasmid was sequenced in both forward and reverse directions using a BigDye terminator cycle sequencing reaction kit v3.1 to confirm that there were no PCR errors. The cDNAs of CYP2C19*1C, CYP2C19*18 and CYP2C19*19 were constructed with a QuikChange multisite-directed mutagenesis kit according to the manufacturer's instructions using the primers as described previously [24]. All CYP2C19 plasmids were sequenced to confirm successful mutagenesis. The cDNAs of CYP2C19*1C, CYP2C19*18 and CYP2C19*19 were subsequently subcloned into the pGYR1 yeast expression vector.

Expression of CYP2C19 enzymes. The pGYR1 vectors containing CYP2C19 cDNAs were used to transform *Saccharomyces cerevisiae* AH22 by the lithium acetate method, and yeast transformants were cultivated [27]. Microsomes from yeast cells were prepared as described previously [28], and stored at −80° until use. Protein concentrations were determined by the method of Lowry *et al.* [29], using bovine serum albumin as a standard.

Assay for CYP2C19 holo- and apoproteins. Microsomal fractions were diluted to a protein concentration of 10 mg/ml with 100 mM potassium phosphate buffer (pH 7.4) containing 20% (v/v) glycerol and 0.4% (w/v) Emulgen 911, and total functional CYP2C19 protein levels were determined by the method of Omura & Sato [30]. Total CYP2C19 protein levels of holo- and apoforms in yeast cell microsomes were determined by immunoblotting. Microsomal fractions (10 µg protein) were separated by 10% SDS-PAGE [31] and electrotransferred to a polyvinylidene fluoride sheet as described by Towbin *et al.* [32]. The sheet was incubated with rabbit anti-human CYP2C19 antibody (diluted at 1:2000) as the primary antibody and then with peroxidase-conjugated goat anti-rabbit immunoglobulin (diluted at 1:5000) as the secondary antibody. Immunoreactive proteins were visualized with chemifluorescence (enhanced chemiluminescence-plus reagents), and the band densities were relatively determined with Scion Image v4.03 (Scion Corporation, Frederick, MD, USA).

Assay for omeprazole 5-hydroxylation. Omeprazole 5-hydroxylation activities were determined by measuring the formation of 5-hydroxyomeprazole according to the methods reported previously [33–35] with some modifications. The incubation mixture contained omeprazole as a substrate (0.2–20 µM), microsomes from yeast cells (500 µg protein/ml) and an NADPH-generating system (1 mM $NADP^+$, 10 mM glucose 6-phosphate, 2 U/ml glucose 6-phosphate dehydrogenase and 5 mM $MgCl_2$) in 50 mM potassium phosphate buffer (pH 7.4) in a final volume of 500 µl. Omeprazole was dissolved in methanol/dimethyl sulfoxide (50:50, v/v). The final concentration of organic solvent (methanol and dimethyl sulfoxide) in the incubation mixture was 1%. The reaction was initiated by the addition of the NADPH-generating system after pre-incubation at 37° for 1 min. After incubation at 37° for 10 min., the reaction was terminated by the addition of 0.1 ml of 0.5 M disodium hydrogenphosphate and 4 ml of dichloromethane/acetonitrile (90:10, v/v). The incubation mixture was spiked with 20 nmol of lansoprazole as an internal standard and vigorously vortexed for 2 min. After centrifugation at 2000 ×g for 15 min., the organic phase was evaporated to dryness under a gentle stream of nitrogen at 35°. The residues were dissolved in 200 µl of 20 mM disodium hydrogenphosphate/methanol (50:50, v/v) and analysed by high-performance liquid chromatography (HPLC). The HPLC system consisted of an L-2130 pump (Hitachi, Tokyo, Japan), an L-2300 column oven (Hitachi) and an L-2400 ultraviolet (UV) detector (Hitachi) equipped with an Inertsil ODS-80A column (4.6 mm i.d. ×150 mm; GL Sciences, Tokyo, Japan). The column was maintained at 40°. Data acquisition was accomplished using D-2000 v1.1 software (Hitachi). Elution was performed isocratically with 20 mM phosphate buffer (pH 6.8)/acetonitrile (72:28, v/v) at a flow rate of 1.0 ml/min. UV detection absorbance was recorded at 302 nm. Standard curve samples were prepared in the same manner as incubation samples. Under these conditions, the retention times of 5-hydroxyomeprazole, omeprazole and lansoprazole were 3.6, 10.5 and 21.4 min., respectively. The recoveries of 5-hydroxyomeprazole and lansoprazole were both >95%. The limit of detection of 5-hydroxyomeprazole (signal-to-noise ratio of 3) was 10 pmol/assay. The 5-hydroxyomeprazole formation was almost linear for microsomal protein concentrations up to 1000 µg protein/ml and for incubation times up to 20 min. at low (0.2 µM) and high (20 µM) substrate concentrations in yeast cells expressing wild-type CYP2C19. Intra- and inter-day variation coefficients did not exceed 10% in any assay.

Data analysis. Kinetic parameters such as K_m and V_{max} for omeprazole 5-hydroxylation were estimated by analysing Michaelis-Menten plots using Prism v5.01 software (GraphPad Software, San Diego,

© 2008 The Authors
Journal compilation © 2008 Nordic Pharmacological Society.

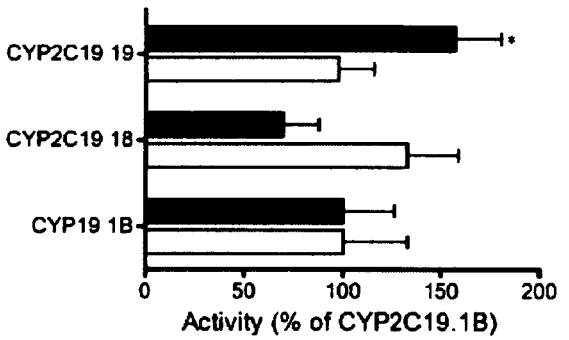

Fig. 2. Omeprazole 5-hydroxylation in microsomes from yeast cells expressing wild-type and variant CYP2C19s. The substrate concentration used was 2 μM. The results are expressed as a percentage of the activity of CYP2C19.1B. The activities of CYP2C19.1B on the basis of microsomal and cytochrome P450 (CYP) protein levels were 74.9 ± 24.8 pmol/min./mg protein and 4.69 ± 1.23 pmol/min./pmol CYP, respectively. Each column represents the mean ± S.D. of three separate experiments derived from independent preparations. □, activity on the basis of microsomal protein level; ▩, activity on the basis of CYP protein level. *Significantly different from CYP2C19.1B ($P < 0.05$).

CA, USA). Intrinsic clearance values were determined as the ratio of V_{max}/K_m. All values are expressed as the mean ± S.D. of three independent transfection experiments. Statistical comparisons were performed by one-way ANOVA with Dunnett's *post hoc* test using Prism v5.01 software. Differences were considered statistically significant when the P value was <0.05.

Results

CYP2C19 cDNAs of wild-type (CYP2C19*1C) and variants (CYP2C19*18 and CYP2C19*19) were constructed, and the corresponding CYP2C19 enzymes (CYP2C19.1B, CYP2C19.18 and CYP2C19.19) were heterologously expressed in yeast cells. In our previous study [24], the reduced CO difference spectra of CYP2C19.1B, CYP2C19.18 and CYP2C19.19 proteins showed a Soret peak at around 450 nm. CYP levels in yeast cell microsomes expressing CYP2C19.1B, CYP2C19.18 and CYP2C19.19 were 15.6 ± 2.4, 30.5 ± 1.8 and 10.1 ± 1.6 pmol/mg protein, respectively. The expression levels of wild-type and variant CYP2C19 proteins in yeast cell microsomes were also assessed by immunoblotting that recognized both holo- and apoforms. The stained bands of CYP2C18.18 and CYP2C19.19 were 171 ± 10 and 56.7 ± 11.8% of CYP2C19.1B, respectively.

Omeprazole 5-hydroxylation activities in yeast cell microsomes expressing wild-type and variant CYP2C19s were then examined. No activity in microsomes of the negative control (mock) was detected at any substrate concentration examined. Fig. 2 shows the levels relative to the activity of CYP2C19.1B at a single substrate concentration (2 μM). The activities of CYP2C19.1B on the basis of microsomal and functional CYP protein levels were 74.9 ± 24.8 pmol/min./mg protein and 4.68 ± 1.23 pmol/min./pmol CYP, respectively. The activity of CYP2C19.18 was not significantly different from that of CYP2C19.1B in any unit term. The activity of CYP2C19.19 on the basis of the microsomal protein level was comparable to that of CYP2C19.1B, whereas activity on the basis of the CYP level was significantly higher (1.5-fold) than that of CYP2C19.1B.

Kinetic analysis of omeprazole 5-hydroxylation was performed to obtain further information on the metabolic ability of variant CYP2C19s as well as wild-type CYP2C19 towards omeprazole. Non-linear regression curves of Michaelis–Menten kinetics are shown in fig. 3, and the calculated kinetic parameters are summarized in table 1. The K_m value for omeprazole 5-hydroxylation of CYP2C19.1B was 1.46 ± 0.24 μM. The K_m value of CYP2C19.19 was significantly higher (1.5-fold) than that of CYP2C19.1B, whereas no significant difference was observed in K_m values between CYP2C19.1B and CYP2C19.18. V_{max} and V_{max}/K_m values for omeprazole 5-hydroxylation of CYP2C19.1B on the basis of microsomal protein level were 130 ± 47 pmol/min./mg protein and 86.6 ± 19.3 μl/min./mg protein, respectively. When activities were normalized to CYP levels to assess the intrinsic function of wild-type and variant CYP2C19 enzymes, V_{max} and V_{max}/K_m values of CYP2C19.1B were 8.09 ± 2.34 pmol/min./pmol CYP and 5.45 ± 0.94 μl/min./pmol CYP, respectively. V_{max} and V_{max}/K_m values of

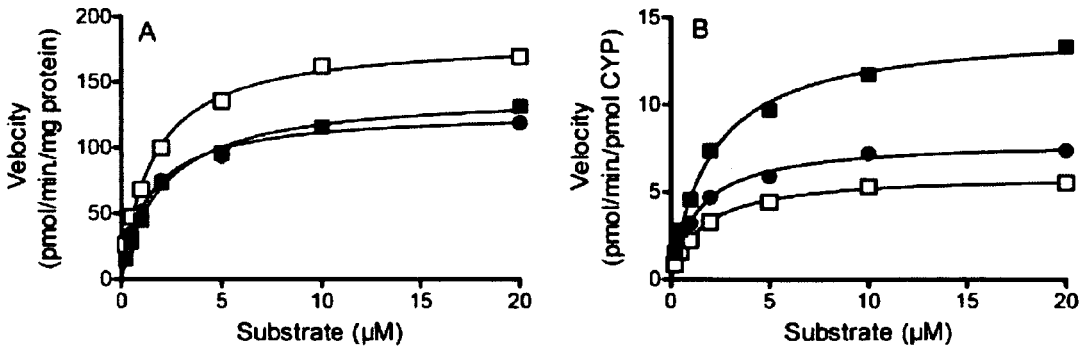

Fig. 3. Michaelis–Menten plots for omeprazole 5-hydroxylation by microsomes from yeast cells expressing wild-type and variant CYP2C19s. (A) Results on the basis of microsomal protein level. (B) Results on the basis of functional cytochrome P450 (CYP) protein level. The substrate concentrations used were 0.2–20 μM. Each point represents the mean of three separate experiments derived from independent preparations. ●, CYP2C19.1B; □, CYP2C19.18; ■, CYP2C19.19.

© 2008 The Authors
Journal compilation © 2008 Nordic Pharmacological Society.

Table 1.

Kinetic parameters for omeprazole 5-hydroxylation by microsomes from yeast cells expressing wild-type and variant CYP2C19s.

		V_{max}		V_{max}/K_m	
Variant	K_m (μM)	Protein (pmol/min./mg protein)	CYP (pmol/min./pmol CYP)	Protein (μl/min./mg protein)	CYP (nl/min./pmol CYP)
CYP2C19.1B	1.46 ± 0.24	130 ± 47	8.09 ± 2.34	86.6 ± 19.3	5.45 ± 0.94
CYP2C19.18	1.66 ± 0.20	186 ± 33	6.07 ± 1.12	112 ± 12	3.65 ± 0.49
CYP2C19.19	2.14 ± 0.32[1]	144 ± 21	14.6 ± 3.5[1]	67.5 ± 10.2	6.75 ± 0.87

Each value represents the mean ± S.D. of three separate experiments derived from independent preparations.
[1]Significantly different from CYP2C19.1B ($P < 0.05$).

CYP2C19.18 were not significantly different from those of CYP2C19.1B in any unit term. The V_{max} value of CYP2C19.19 on the basis of the microsomal level was comparable to that of CYP2C19.1B, whereas the value on the basis of CYP protein level was significantly higher (1.8-fold) than that of CYP2C19.1B; however, no significant differences in V_{max}/K_m values were observed between CYP2C19.1B and CYP2C19.19 in any unit term.

Discussion

Omeprazole is one of the most widely used proton pump inhibitors for the treatment of gastric acid-related disorders [1,2]. Previous reports have suggested that CYP2C19 plays an important clinical role in the metabolism of omeprazole [11,16]. Since the *CYP2C19* gene is highly polymorphic and shows marked interethnic differences [11,16], it is important to clarify its effect on the metabolism of omeprazole for individual drug therapy. We recently identified two *CYP2C19* allelic variants (*CYP2C19*18* and *CYP2C19*19*) causing amino acid substitutions in a Japanese population [23], and analysed their metabolic ability towards *S*-mephenytoin as a typical substrate for CYP2C19 [24]. In this study, omeprazole 5-hydroxylation in microsomes from yeast cells expressing wild-type and variant CYP2C19s was investigated.

As reported previously [24], we confirmed the expression of CYP holo- and apoproteins of CYP2C19.1B, CYP2C18.18 and CYP2C18.19 by reduced CO difference spectral and immunoblot analyses. The level of CYP2C19 holoproteins of CYP2C19.18 was significantly higher than that of CYP2C19.1B, whereas the level of CYP2C19.19 was significantly lower than that of CYP2C19.1B. The expression levels of CYP2C19 protein in yeast cells may differ among wild-type and variant CYP2C19s due to altered stability or folding efficiency of the proteins.

Li *et al.* [8] estimated by the relative activity factor that the contribution of CYP2C19 to omeprazole 5-hydroxylation is 89- 41%, suggesting the importance of CYP2C19 in omeprazole metabolism; therefore, we examined the effect of *CYP2C19*18* and *CYP2C19*19* on omeprazole 5-hydroxylation using recombinant CYP2C19 enzymes expressed in yeast cells. Enzymatic activities were analysed in this study in two ways: as pmol/min./mg protein (on the basis of the microsomal protein level) to consider the efficiency of the mutant expression, and as pmol/min./pmol CYP (on the basis of the CYP protein level) to assess the function of each mutant protein. Both variant CYP2C19s were capable of catalyzing omeprazole 5-hydroxylation as well as wild-type CYP2C19 at the substrate concentrations examined, and the kinetics of all CYP2C19 enzymes fitted a typical Michaelis-Menten model. The K_m value for omeprazole 5-hydroxylation of wild-type CYP2C19.1B having Ile/Val in this study was comparable to other studies in an expression system using yeast or human B-lymphoblastoid cells [7,8]. The K_m value of CYP2C19.19 having Ser51Gly/Ile331Val was significantly higher than that of CYP2C19.1B, although the relative level was 1.5-fold. Since the V_{max} value of CYP2C19.19 on the basis of the CYP protein level was 1.8-fold higher than that of CYP2C19.1B, the V_{max}/K_m value was consequently comparable to wild-type CYP2C19. In contrast, K_m, V_{max} and V_{max}/K_m values of CYP2C19.18 having Arg329His/Ile331Val were similar to those of CYP2C19.1B, suggesting that Arg329His substitution hardly affects omeprazole 5-hydroxylation. It has been suggested that *S*-mephenytoin 4′-hydroxylation is a typical probe for CYP2C19 [36,37]. Recently, we reported that the increase in K_m value for *S*-mephenytoin 4′-hydroxylation is observed with CYP2C19.19 but not with CYP2C19.18; therefore, we consider that Ser51Gly substitution in CYP2C19.19 decreases the affinity towards substrates for the CYP2C19 enzyme. Further studies are required to identify the mechanism of interaction between enzymes and substrates for CYP2C19.

In conclusion, we expressed two variant CYP2C19 enzymes with amino acid substitutions (CYP2C19.18 and CYP2C19.19) found in a Japanese population as well as wild-type CYP2C19 (CYP2C19.1B) in yeast cells, and the kinetics of omeprazole 5-hydroxylation were determined. The values of K_m and V_{max} on the basis of the CYP level for omeprazole 5-hydroxylation of CYP2C19.19 exhibited higher values than those of CYP2C19.1B, although no significant difference in the V_{max}/K_m value on the basis of microsomal or functional CYP protein level was observed between CYP2C19.1B and CYP2C19.19. In contrast, K_m, V_{max} and V_{max}/K_m values of CYP2C19.18 were similar to those of CYP2C19.1B. These findings suggest that Ser51Gly substitution in CYP2C19.19 decreases the affinity towards substrates for the CYP2C19 enzyme, and may mean that *CYP2C19*19* allele leads to variations in the clinical response to omeprazole.

© 2008 The Authors
Journal compilation © 2008 Nordic Pharmacological Society.